Development and Evaluation of a Quick Release Posterior Strut Ankle Foot Orthosis

Wentao Li

Thesis submitted to the Faculty of Engineering
in partial fulfillment of the requirements for the degree of

MASTER OF APPLIED SCIENCE

in Mechanical Engineering

University of Ottawa
Ottawa, Ontario

October 2020

Abstract

Ankle foot orthosis (AFO) stiffness affects ankle range of motion but can also provide energy storage and return to improve mobility. To perform multiple activities during the day, a person may want to change their AFO stiffness to meet their activity's demand. Carrying multiple AFO and changing the AFO is inconvenient and could discourage users from engaging in multiple activities. This thesis developed a new quick-release mechanism (QRM) that allows users to easily change posterior strut elements to change AFO stiffness. The QRM attaches to the AFO and requires no tools to operate. The new QRM includes a quick-release key, weight-bearing pin, receptacle anchor, and immobilization pin. A prototype was modelled with SolidWorks and simulated with SolidWorks Simulation. The QRM was designed to have no mechanical failure during intense activities such as downhill walking and running. Unlike a solid screw connection, the QRM needed an additional part to eliminate unsecured motion related to clearance between the quick release key and receptacle anchor. Mechanical test results and measurement data demonstrated no deformation on each part after mechanical testing. User testing revealed that, although the quick release mechanism can be locked or unlocked rapidly, the person's posture when operating can facilitate strut swapping. A learning effect occurred by repeated practice. The Quick Release AFO (QRAFO) prototype verified the manufacturing feasibility of the QRAFO design. Overall, the novel quick release AFO improved strut swapping time without sacrificing device strength.

Table of Contents

Table of Figures

List of Tables

Definitions

Anterior	To the front of the body
Centre of mass	Point representing a body's mean position of mass
Distal	Away from the rest of the body
Dorsiflexion	Foot rotation towards the knee
Eversion	Foot rotation away from the midline of the body
External moment	Moment applied from outside the body
Gait cycle	Interval between any repetitive events of walking
Frontal plane	Divides the body into front and back (aka, coronal plane)
Ground reaction force	Reaction force from the ground applied to the foot
Internal moment	Moment generated by muscles and/or ligaments
Internal rotation	Rotation about long axis, with anterior surface moving medially
Inversion	Foot rotation towards the midline of the body
Kinematics	Joint or body segment movements
Kinetics	Forces and moments that produce movement
Lamination	A laminated structure of carbon fibre fabrics
Lateral	Away from the midline of the body
Medial	Towards the midline of the body
Orthosis	Assistive device that supports, aligns, prevents, or corrects deformities or improves movement
Plantarflexion	Foot rotation away from the knee
Posterior	To the back of the body
Proximal	Towards the rest of the body
Power	Rate at which work is done or energy is expended
Sagittal plane	Divides the body intro right and left
Stance	Gait cycle phase when foot contacts the support surface
Step	Foot strike of one extremity to foot strike of opposite extremity
Stride	Foot strike of one extremity to next foot strike of same extremity
Swing	Gait cycle phase without foot contact on the support surface
Transverse plane	Divides the body into upper and lower

Abbreviations

AFO	Ankle-foot orthosis
AAFO	Active ankle-foot orthosis
CFAFO	Carbon fibre ankle-foot orthosis
COM	Centre of mass
FEA	Finite element analysis
GRF	Ground reaction force
IDEO	Intrepid Dynamic Exoskeleton Orthosis
IM-pin	Immobilization pin
MR	Magnetorheological
MSAFO	Multiple stiffness ankle-foot orthosis
PCC	Pearson correlation coefficients
PDEAFO	Posterior dynamic element ankle-foot orthosis
PLSAFO	Posterior leaf spring ankle-foot orthosis
QRAFO	Quick release ankle-foot orthosis
QRM	Quick release mechanism
QTCL	Quarter-turn cam lock
QTF	Quarter-turn fastener
ROM	Range of motion
SEA	Series elastic actuator
SLM	Sliding locking mechanism
Ti-pin	Titanium pin
TOHRC	The Ottawa Hospital Rehabilitation Centre

Acknowledgments

First of all, I would like to thank my two supervisors, Dr. Natalie Baddour & Dr. Edward Lemaire for all of their guidance, support, and encouragement throughout my research.

A thank you also goes out to the following individuals:

Staff of Rehabilitation Technology Lab
Staff of Prothetics and Orthotics Department
Staff of Brunsfield Center

Finally, thank you to my family and friends.

Chapter 1: Introduction

Ankle foot orthoses (AFO) are mobility enhancement devices that assist people with gait disabilities. AFO functions evolved from assisting foot drop to providing gait control, thereby enhancing walking and standing ability. One recent advancement in AFO design uses a posterior strut element that can store and return energy during movement. An off-loading cuff reduces weight bearing on the foot and ankle, thereby allowing users with ankle disabilities to engage in more intense activities such as running and uneven road walking. Orthotists can customize a device by selecting strut stiffness to correspond to the user's activity level and body weight. However, a stiffer device limits the ability to perform some activities that require ankle range of motion beyond the strut material deformation, such as casual walking and driving. Currently, there is no available AFO that allows a person to switch AFO stiffness to match different activities, other than carrying multiple devices and then changing to a completely different AFO.

In this thesis, a new quick-release ankle-foot orthosis (QRAFO) was proposed to provide a solution that allows users to change device stiffness to better accommodate a range of physical activities. A preliminary FEA simulation on design safety was performed, followed by mechanical evaluations to verify mechanical performance on running loads and downhill walking loads. Lastly, a quick release mechanism (QRM) functional test was designed to assess the strut swap time with comparison of strut swap time with a screw-anchor connection used in the Posterior Dynamic Element Ankle-foot Orthosis (PDEAFO, Figure 1-1).

Figure 1-1 Posterior Dynamic Element Ankle-foot Orthosis. Adapted from [1]

1.1 Rationale

Users participating in different activities require different AFO stiffness. Current posterior strut AFO designs, including the Intrepid Dynamic Exoskeleton Orthosis (IDEO) and the Posterior Dynamic Element Ankle-foot Orthosis (PDEAFO), allow an orthotist to select a strut with

appropriate stiffness, based on user activity level and body weight. Since the strut is connected to the foot and shank parts by lock-tightened screws, users cannot easily swap struts during the day. Although the modularized design helps users to select the most appropriate stiffness for daily use, the need to change device stiffness between activities has not been addressed to date. For example, a user still needs to remove their device while driving to allow for more ankle motion.

A device with a changeable stiffness would assist the user to better engage in different activities. Section 2.5 reviews many active AFO approaches to change stiffness during activities. Most active AFOs only consider stiffness control during a walking gait.

The current modularized design of a posterior strut AFO can be utilized and improved to achieve multiple stiffnesses among multiple needs, by redesigning the ankle joint connection such that it enables fast swapping.

1.2 Objectives

The objectives of this thesis are:

1. Design a quick release mechanism that replaces the current PDEAFO anchor system.
2. Evaluate quick release mechanism mechanical properties:
    a. Overall strength under running load and downhill walking load.
    b. Evaluate connection strength under running and downhill walking loads.
3. Evaluate quick-release mechanism efficiency for reducing strut-swap time.
4. Verify the manufacturing feasibility of QRAFO.

1.3 Thesis contributions

The principal contribution of the thesis was creating and validating a QRAFO that provides appropriate device stiffness, thereby providing better energy storage and return during different activities for PDEAFO users.

Specific thesis contributions are:

1. Designing a viable quick release mechanism for a posterior strut AFO.
2. Demonstrating that the new design can accommodate running and downhill walking loads.
3. Evaluating the quick release mechanism function and determining that posterior struts on a 3D printed prototype can be swapped in less than 10 seconds.
4. Creating a complete carbon fibre QRAFO, thereby verifying the fabrication process that will be used by orthotists and orthotic technicians.

1.4 Thesis outline

This thesis is divided into eight chapters. Chapter 2 is a literature review covering ankle function during gait, state of the art in ankle-foot orthoses, and AFO effects on gait. Chapter 3 presents the QRAFO design criteria. Chapter 4 introduces the quick-release mechanism design; including, design concept development, QRAFO prototype, formulation to avoid component fatigue, FEA evaluation on strength under fatigue, peak running load, and peak downhill walking load. Chapter 5 presents the quick release mechanism mechanical evaluation with running and downhill walking load. Chapter 6 performs functional analysis of a 3D printed QRAFO with able bodied participants. Chapter 7 concludes the fabrication process of the QRAFO and validates the process with a QRAFO prototype. Chapter 8 concludes the thesis and outlines future work on the QRAFO.

Chapter 2: Literature Review

This chapter reviews biological ankle-foot mechanics and ankle-foot orthoses, to better determine design criteria and gain insight regarding ankle-foot orthosis effects on gait.

2.1 Gait cycle

The ankle joint complex is located between the lower leg and the foot and forms the kinetic linkage allowing interaction between the lower limb and ground [2]. The ankle plays a vital role in weight-bearing during gait while also providing stability [3]. Twenty-six individual bones with thirty-three joints function simultaneously to control the ankle motion on three anatomical planes (Figure 2-1).

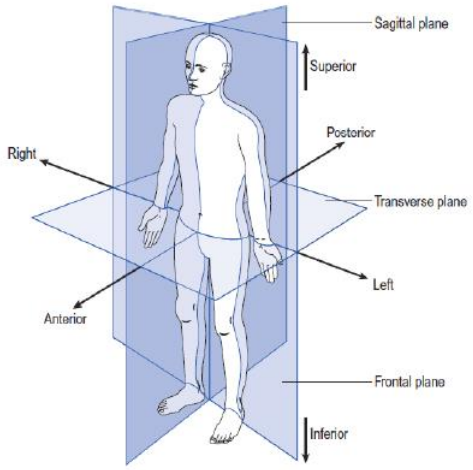

Figure 2-1 Three anatomical planes (sagittal, frontal, transverse) and six directions (left, right, anterior, posterior, superior, inferior). Adapted from [4].

A walking gait cycle can be defined from one-foot landing to the same foot contacting the ground again (i.e., stride), with this cycle divided into stance and swing phases (Figure 2-2). Stance phase is the period with foot-ground contact, with five subphases: initial contact, loading response, mid-stance, terminal stance, pre-swing. The swing phase has three sub-phases: initial swing, mid-swing, terminal swing.

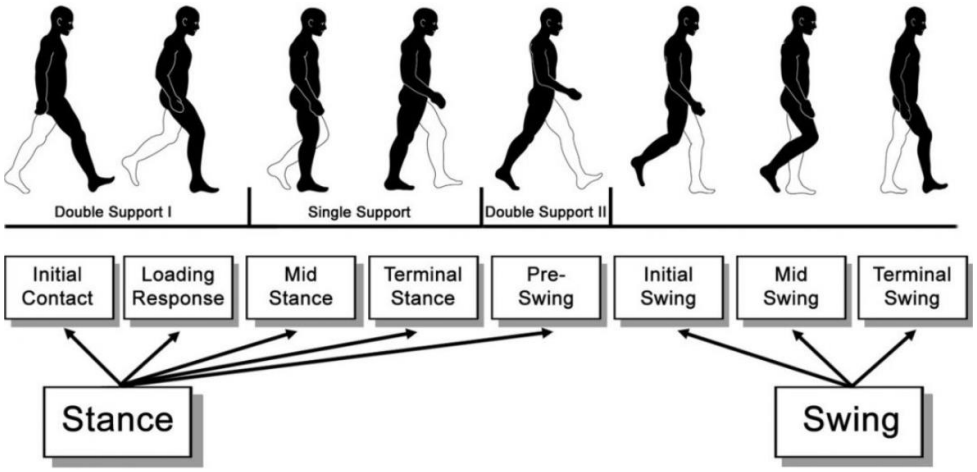

Figure 2-2 Gait cycle and phases. Adapted from [5].

2.2 Ankle kinematics and kinetics during gait

Three key pairs of ankle movements occur on three anatomical planes, plantarflexion and dorsiflexion in the sagittal plane, abduction and adduction in the transverse plane, and inversion and eversion in the frontal plane (Figure 2-3, Table 2-1) [3].

Figure 2-3 Ankle motion in three anatomical planes (Adapted from [3]).

2.2.1 Range of motion

Ankle range of motion (ROM) is an important kinematic parameter during gait. Ankle motion occurs primarily in the sagittal plane, with plantarflexion and dorsiflexion. Maximum sagittal plane ROM ranges from 65 to 75°, with 40-55° plantarflexion and 10-20° dorsiflexion [3]. Frontal plane ROM ranges from 23 of inversion to 12 of eversion [3].

Sagittal ROM during daily activities is much smaller than the full range, with approximately 30° for walking [3]. Ankle sagittal plane ROM consists of controlled plantarflexion at initial contact to maximum dorsiflexion during terminal stance, up to 15º, rapid plantarflexing to a peak of 18º at toe-off, and controlled dorsiflexion during swing, for a total ROM of approximately 33º (Figure 2-4).

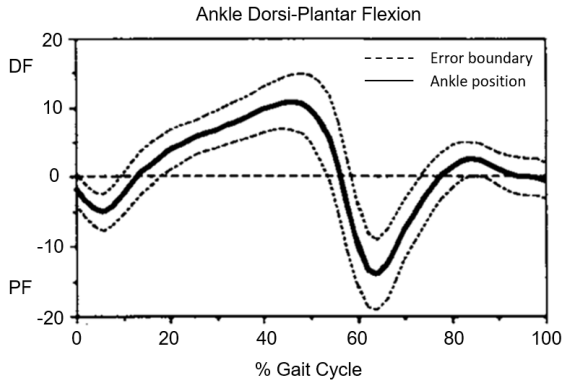

Figure 2-4 Ankle dorsiflexion and plantarflexion during one gait cycle. Adapted from [6].

2.2.2 Moment and power

Figure 2-5 shows sagittal plane ankle moment and power for one gait cycle. Small dorsiflexion moments and powers occur after initial contact due to heel strike [4]. Ankle plantarflexion moments increase continuously throughout midstance and into late terminal stance, when foot push-off begins with plantarflexion moment decreasing rapidly until toe-off. The largest moment occurs at terminal stance phase (approximately 1.6 Nm/kg) [7]. Mild dorsiflexion moments occurs throughout swing phase to control foot angle and maintain foot-ground clearance [4], [7]. Gait cycle power curves show energy peak requirements at terminal stance when push-off happens. This rapid push-off is the largest power generation phase of all lower limb joints [7].

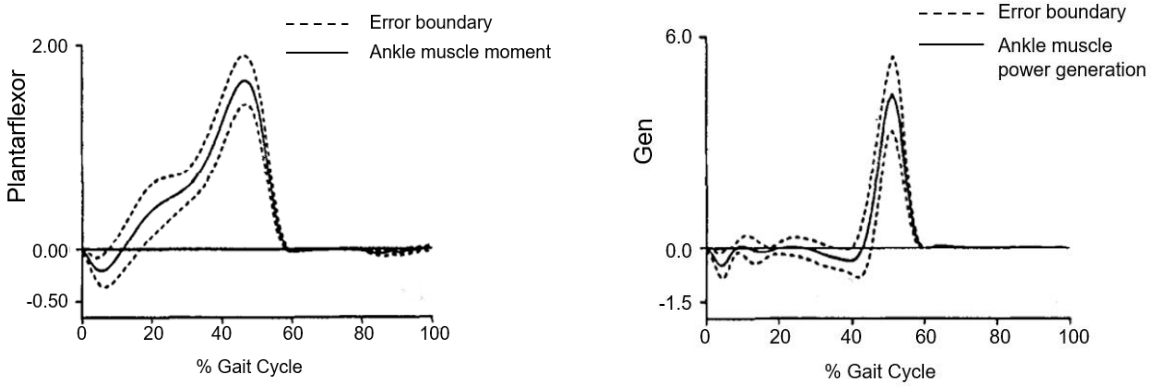

Figure 2-5 Sagittal ankle moment (Nm/kg, left) and power (J/kg, right). Adapted from [7].

Table 2-1 Gait function and ankle motion for each phase of normal walking [4]

	Subphase	% Gait	Ankle motion	Function
Stance	Initial contact	0-10	Neutral	Dorsiflexors are active to resist plantarflexion to avoid foot slap, and plantarflexion begins
	Loading response	10-12	Plantarflexion and subsequent dorsiflexion	Dorsiflexors control ankle rotation to smooth plantarflexion to foot flat and then assist dorsiflexion to midstance
	Mid-stance	12-32	Dorsiflexion	Dorsiflexor moments assist ankle rotation to mid-stance and then eccentric plantarflexor moments control shank rotation over the foot
	Terminal stance	32-50	Dorsiflexion and subsequent plantarflexion	As the heel rises, the toes remain flat on the ground and ankle continues rotation to peak dorsiflexion, plantarflexors maintain the ankle angle as the knee begins to flex, ankle rotates into plantarflexion in late terminal stance
	Pre-swing	50-60	Plantarflexion	Plantarflexors rapidly plantarflex the ankle, producing a forward horizontal reaction force to advance the body
Swing	Initial swing	60-77	Dorsiflexion	Foot leaves the ground with maximum plantarflexion and dorsiflexors lift toes and hold the foot in dorsiflexion, maintaining foot-ground clearance
	Mid-swing	77-86	Neutral	Dorsiflexors continue to contract mildly to maintain a neutral position for toe-ground clearance
	Terminal swing	86-100	Neutral	Dorsiflexor contractions increase to hold the ankle in position, in anticipation of the greater forces needed during loading response

2.3 Ankle foot orthosis

Ankle foot orthoses (AFO) are assistive devices that control ankle motion and provide stability for people with limb weakness or spasticity. AFO differ by materials, joint connection, geometry, and power condition [8]. Generally, AFO can be classified as passive, semi-active, and active. Semi-active and active AFO have actuators, power sources, and control systems, with direct or indirect motion control. Although semi-active and active AFO can adapt ankle rotation control during gait, passive AFO are the most popular device due to the lower cost, smaller size, lighter weight, and many other benefits [9].

2.3.1 Traditional passive AFO

Passive AFO is the most common AFO and addresses abnormal gait due to ankle dysfunction. Passive AFO are usually worn by people with lower limb paralysis (stroke, etc.) [10], neuromuscular disease resulting in lower limb weakness (foot drop, etc.), and spasticity that holds the foot and ankle in biomechanically poor positions and limits movement (cerebral palsy, etc.) [11].

Two classic passive AFOs are the articulated AFO and non-articulated AFO (also called rigid AFO). Articulated AFOs are usually hinge connected with a defined motion range. Non-articulated AFO is usually a piece of material [10], or several materials, connected rigidly.

Non-articulated AFOs are traditionally fabricated from thermoplastics to allow for easy modification, although carbon fibre devices are becoming common as prefabricated devices and for user's some special needs. The footplate trimline, proximal border, and proximal closure strap can be adjusted to modify focal force locations, changing the stabilizing bending moments [12]. Frontal plane motion is limited via localizing medial-lateral AFO forces, proximal and distal to the malleoli. For increased stability against foot inversion/eversion, the anteroposterior and footplate trimlines can be extended [12]. Articulated AFO can resist plantarflexion during swing phase to prevent foot drop and provide some free ankle motion during stance.

Both rigid or articulated AFO can appropriately control ankle motion, thereby increasing dorsiflexion at initial contact and swing phase for people with ankle dysfunction [13]–[17]. More dorsiflexion during stance phase occurs when wearing a hinged AFO than a rigid AFO [17], [18]. Ankle plantarflexion moment is significantly increased in loading response and ankle dorsiflexion moment is decreased in terminal stance with articulated AFO, compared with the rigid AFO [17].

(a) (b)

Figure 2-6 (a) Thermoplastic rigid AFO, (b) flexor joint articulated AFO. Adapted from [19]

2.3.2 Posterior leaf spring AFO

The posterior leaf spring (PLS) AFO features shallow medial and lateral trimlines, [12], [20], [21], thereby providing more flexibility in the sagittal plane. The traditional PLSAFO is fabricated from thermoplastic (Figure 2-7).

Figure 2-7 Posterior leaf-spring AFO. Adapted from [22].

From initial contact to early loading response, the posterior leaf decelerates ankle rotation and minimizes foot slap. In mid-stance, the leaf spring permits controlled dorsiflexion through large material deformation, providing smooth tibia advancement until late stance [12]. During terminal stance, as plantar flexor begins, energy stored in the leaf spring releases and assists push-off. The posterior leaf spring resists plantarflexion, holding the foot in slight dorsiflexion, during swing phase. A small amount of ankle rotation can occur during swing, dependent on thermoplastic thickness and posterior strut trimlines [12].

2.3.3 Carbon fibre AFO

Although some PLSAFO designs can assist plantarflexion and allow dorsiflexion, push-off assistance is minimum [23]. Therefore, PLSAFO designs were adapted to incorporate carbon fibre materials to provide enhanced energy storage from loading response through midstance and energy release from terminal stance to preswing [12], [24], [25]

The carbon fibre spring is typically L-shaped, with the base attached to the plantar surface of the footplate and the upright attached to the posterior surface of the proximal cuff [12]. Compared with thermoplastic AFO, the carbon fibre strut's increased stiffness requires more force to deform and returns greater force as the AFO returns to its original shape. The orthotist selects carbon fibre

spring stiffness based on the person's weight and activity level. Carbon fibre AFO (CFAFO) can also be prefabricated devices, such as Össur AFO Light (Figure 2-8).

Figure 2-8 Carbon fibre strut AFO (left), Össur AFO Light (right). Adapted from [24], [26].

Carbon fibre AFO typically enhance gait control and improve biomechanical outcomes [24], [25], [27]–[29]. Compared with traditional PLSAFO, the CFAFO significantly increased ankle ROM, ankle angular velocity, and power generation at pre-swing [24], [25], [28]. Improved push-off was achieved by AFO energy storage through loading response and midstance, resulting in a forward push of the shank during terminal stance, thereby increased push-off [28]. Bartonek et al. reported increased positive work at the ankle when wearing a carbon fibre AFO, compared with regular thermoplastic AFO (from 0.06 to 0.09 J/kg). These results were still much lower than able-bodied gait (0.25 J/kg) [29].

2.4 Posterior strut AFO

People suffering from limb salvage injuries may be unable to perform intense activities with a typical plastic AFO due to insufficient energy storage and return [23]. This class of AFO are worn by people with excessive ankle and foot pain that requires foot unloaded during stance and people with volumetric muscle loss that requires energy storage and return during push off (military personnel who have under gone limb salvage, etc.) [23], [30].

Though CFAFO designs improve gait and provide more energy return during push-off, the energy return was insufficient for high-active activities such as running and jumping [29], [30]. Posterior strut AFO implements a rigid posterior strut as an individual functional component, providing better energy storage and return, facilitating return to high-intensity activities [30], [31].

2.4.1 Intrepid dynamic exoskeletal orthosis (IDEO)

The Intrepid Dynamic Exoskeletal Orthosis (IDEO), developed by the Center for the Intrepid (San Antonio, TX), is a custom, energy-storing device that supports and protects people with lower extremity trauma limb salvage injuries [23]. The IDEO is crafted with three carbon fibre components: ground reaction cuff, mounted posterior strut, and footplate (Figure 2-9). The ground reaction cuff is a circumferential support fashioned in the style of a patellar-tendon-bearing prosthesis, located at the proximal part of the leg with a posterior attachment to the proximal end of the carbon fibre strut [30]. The ground reaction cuff provides off-loading to alleviate ankle pain. The posterior strut can deform to provide energy storage and return. A cushioned heel absorbs shock during loading response. IDEO advanced modular design allows struts changes as strength and motion ability change, and can be easier to don and doff [23], [30].

Jeanne et al. compared the IDEO with a regular CFAFO and PLSAFO. The IDEO significantly improved performance on five training activities: four-square step test, sit-to-stand test, stair ascent, self-selected speed walking on level terrain, self-selected speed rocky terrain, and 40-yard dash [30], [32]. The off-loading cuff reduced ankle pain [31], [32].

Figure 2-9 IDEO orthosis. Adapted from [23].

2.4.2 Dynamic Strut AFO

The Dynamic Strut AFO [33] by Coyote Design (Figure 2-10) combines an energy return strut with custom thermoformed AFO. The combination of thermoplastic and energy return strut provides dorsiflexion or plantarflexion stabilization with energy return for more active people,

thereby covering a wider activity range during daily use. Strut selection is based on user weight and activity level.

Figure 2-10 Dynamic Strut AFO. Adapted from [33].

2.4.3 Posterior Dynamic Element AFO

The Posterior Dynamic Element AFO (Figure 2-11) [1] is another posterior strut AFO that is entirely fabricated from carbon fibre. AFO strut stiffness can be selected to match user activities. The PDE AFO introduced an anchor system by laminating a pre-threaded metal plate within the carbon fibre matrix, thereby facilitating strut adjustment. Similar to the IDEO, PDE AFO provides high energy return and off-loads body weight during intense activities.

Figure 2-11 Posterior Dynamic Element AFO. Adapted from [1].

2.5 Variable stiffness AFO

2.5.1 Series elastic actuation active AFO

A variable-impedance active ankle-foot orthosis (AAFO, Figure 2-12) was proposed by Joaquin et al. [34] to treat drop foot. A thermoplastic articulated AFO was the main body and a series elastic actuator (SEA) connected the proximal cuff and sole. The SEA was located on the posterior sagittal plane that controlled ankle sagittal plane motion [35]. This 2.6kg device controlled ankle rotatory stiffness, thereby providing an adaptive control at each gait phase to enhance walking.

Figure 2-12 SEA adaptive controlled AAFO (Adapted from [36]).

The control policy prevented foot slap from heel strike to midstance. During late stance, the controller minimized impedance to not impede power plantarflexion. In swing phase, impedance was controlled to maintain foot dorsiflexion, preventing toe drag.

2.5.2 Magnetorheological fluid brake AFO

Magnetorheological (MR) fluid brakes have been researched over the last two decades in rehabilitation devices. This type of brake utilizes a liquid state that responds to magnetic fields [37]. Varying the magnetic field provides controllable braking forces, which contribute to variable dampening at the ankle, thereby enable variable resistance at different gait phase. MR fluid brake devices have been reported for ankle-foot orthosis joints [38], [39], knee brace joints [37], and prosthetic joints [41]. Compared with conventional motors, MR fluid brakes have better force control and better energy efficiency [42].

Kikuchi et al. developed a novel variable dampening AFO utilizing MR fluid brake and spring (i-AFO) [39], [43], [44]. The latest i-AFO (Figure 2-13) demonstrated a high torque-to-weight

ratio with 10 Nm maximum output torque on a 237g brake. While preventing foot drop, the MR brake damping effect also controlled ankle rotation during loading response. Generally, the MR brake improved gait patterns for people with abnormal gait [45].

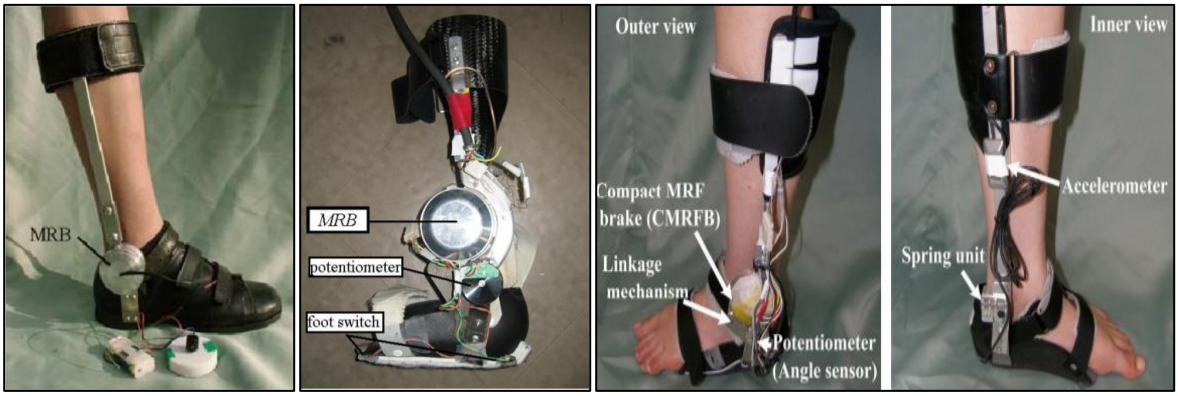

Figure 2-13 Original i-AFO prototype (left), second generation (middle), third generation (right).

2.5.3 Active artificial muscle AFO

Ferris et al. developed a pneumatic artificial muscle AFO (Figure 2-14) to provide ankle torque to assist gait [46]. An active pneumatic tube connected the AFO cuff (anterior) and AFO sole (posterior). An external pump supported the 1.7 kg weight device. Peak dorsiflexion moment was 20.7 Nm and peak plantarflexion moment was 50.7 Nm, 36% of plantarflexor power and 123% of dorsiflexor power [46].

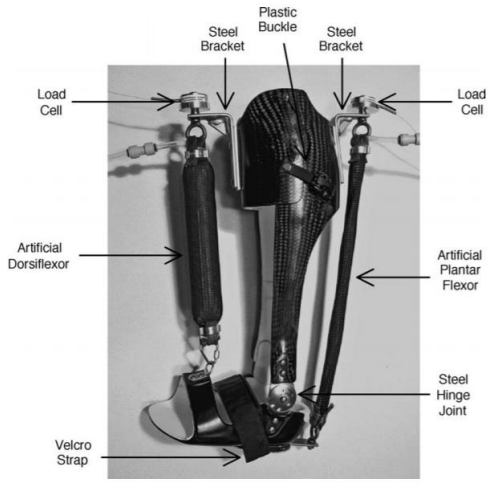

Figure 2-14 Pneumatic actuated AFO. Adapted from [46].

2.6 Summary

An ankle-foot orthosis can improve walking mechanics and safety, thereby improving quality of life. Traditional plastic AFO are widely used because of their low cost, while properly addressing drop-foot and severe ankle instability issues [9]. However, the thermoplastic leaf spring AFO limits ankle movement to achieve these functional benefits [10]. Articulated AFO compensate for this rigid AFO limitation by allowing dorsiflexion during stance [17]. The PLSAFO design limits ankle movement but does provide some dorsiflexion during stance by larger material deformation and superior energy return [47]. Lower than able-bodied energy storage and return during pushoff remains a limitation for both articulated and PLSAFO [23], [30].

Different CFAFO designs can provide a lighter and lower profile device, provide better energy storage and return during terminal stance and pre-swing, or improve knee and ankle stability [27]. The energy storage and return CFAFO design can help people return to more intense activities. Unlike plastic AFO, the CFAFO is hard to adjust (pressure points on limb, leaf spring stiffness, etc.) once the resin has cured [48]. With thermoplastic AFO, orthotists typically adjust the shape during the fitting process for optimal function and comfort

IDEO researchers built a modularized device that allowed physicians to select strut stiffness to match user activity levels [23] and stiffer struts can be selected than regular CFAFO. An off-loading option was also added to the IDEO cuff to reduce pain when performing intense activities [23], addressing active user's needs when returning to their previous activities.

Though the IDEO and posterior strut AFO allow individuals to engage in a broader range of activities, users cannot effectively perform all daily activities with one strut stiffness. Active devices that provide better stiffness control were proposed. MIT's SEA controlled AFO was bulky and heavy compared with other AFO options, which made the SEA device difficult for daily use. The pneumatic artificial muscle AFO provided large force during push-off; however, the need for an external pump made the device not portable. MR fluid breaks provided variable damping control during initial contact, but minimum assistance during push-off [39], [44] and the devices were heavier than other AFO designs.

To better address return-to-activities needs, either a powerful and portable active AFO or a strut switchable posterior AFO may be considered.

Chapter 3: Design Criteria

This chapter presents multiple stiffness AFO (MSAFO) functionality and design criteria. The goal of a MSAFO is to allow an AFO user to change AFO stiffness to improve ankle control performance across daily activities. A quick release AFO (QRAFO) is a MSAFO approach where a posterior strut can be rapidly swapped, thereby changing AFO stiffness.

3.1 Response time

Two types of response times should be considered: material response time and stiffness changing time. Material response time is important and must be faster than the loading response phase. Winter reported average natural cadence for level ground walking to be 105.3 steps/min [49], which implies that the average stride time starting from initial contact to the next foot contact is 1.14 seconds. Weight acceptance task time is approximately 0-12% of the gait cycle [50], which would correspond to approximately 0.14 seconds for natural cadence walking and 0.17 seconds for slow cadence. The delay for the control, including material reaction time and control policy time, should be less than 0.01 seconds.

A person can spend 30 seconds putting on a shoe [51]. With this as a basis, changing stiffness by manually swapping struts should take less than 30 seconds for end-user acceptance.

3.2 Stiffness

A multiple stiffness AFO should provide appropriate ankle stiffness during gait, demonstrated by improved walking range of motion (ROM) and ankle moments. Able-bodied ankle ROM during walking is 10-20° dorsiflexion and 10-15° plantarflexion [3]. The maximum ankle moment in the sagittal plane is 1.6 to 2.0 Nm/kg during walking [52]. For people who lack plantarflexion strength, plantarflexion moments are generated by AFO material deformation energy storage and return. The maximum desired moment from the MSAFO is at least 20% of the maximum ankle moment (0.32 Nm/kg) [52].

3.3 Weight

Device weight is an important design factor for assistive technology. An active AFO has a weight range from 0.86 to 2.6 kg [52], with an average weight of 1.55 kg. For end-user acceptance, the MSAFO should weigh less than 1.5 kg.

The device user's body weight is important for ankle biomechanics and AFO failure. The MSAFO must withstand the force exerted during loading response and other weight-bearing periods. Walpole et al. estimated that an average American weighs 80.7 kg [53]. The U.S. Department of health and human services [54] reported that the average male over 20 years old, between 2011 and 2014, weighed 88.8 kilograms. The 90^{th} percentile of US male weight is 113.3 kg. Meanwhile, the average body mass of US females in the same criterion is 74.7 kg and the 90^{th} percentile of the same criterion is 104.0 kg. Therefore, considering that users may carry backpacks, MSAFO should withstand daily use by a 120 kg person.

3.4 Device lifespan

Daily activities can lead to AFO material fatigue. MSAFO life should be a balance between product cost and device endurance. Consumers are suggested to replace their orthosis every two or three years [55]; therefore, the MSAFO should function appropriately for at least three years of normal usage. A review paper indicated that an average healthy adult takes 4000 to 18000 steps per day, and that 10000 steps/day is a common goal for healthy adults [56]. Therefore, the target life for MSAFO under walking load is approximately 10^7 cycles.

3.5 AFO joint strength

MSAFO will be used for most daily activities, from light activities such as sitting to intense activities such as running. The orthosis must withstand impacts from loading response during intense activities such as running and steep downhill walking. Maximum ground reaction forces (GRF) can reach or surpass three times body weight during running at 5 m/s on level ground [57]–[59]. A 16.5 to 24-degree slope is considered as a strong slope [60]. With this as a basis, MSAFO should be able to support user walking at a 20-degree slope. The peak vertical ground reaction force while descending a 20-degree ramp can be 1.2 times body weight [61].

For highly active users, the AFO can provide offloading at the orthosis cuff, based on user need [1], [23]. The MSAFO design should have the capacity of offloading up to 80 percent body weight during running or downhill walking.

3.6 Design criteria summary

MSAFO design criteria are summarized in Table 3-1.

Table 3-1 MSAFO design criteria

Objective	Criteria
Function	Stiffness changed automatically or manually
User weight range	Maximum 120 kg
AFO weight	Maximum 1500 g
Range of motion	-15 to 20 degrees
Peak moment generated by AFO	0.32 Nm/kg
AFO endurance	10^7 gait cycles

Chapter 4: Quick Release Posterior Strut Ankle Foot Orthosis Design

A quick-release approach is proposed to enable posterior-strut AFO users to efficiently swap struts to change AFO stiffness and better accommodate multiple activities during daily living, thereby providing a MSAFO. The quick release AFO (QRAFO) design is based on the PDEAFO concept (Chapter 2.4.3). To enable quick release and swapping, a novel quick-release mechanism (QRM) was developed.

This chapter presents the process of designing the quick-release posterior strut ankle-foot orthosis; including, how the QRM design relates to the design criteria, three design ideas, and a scoring scheme based on desired functions to select the QRM design approach. A prototype QRAFO is described and simulation and mechanical analyses on the QRM are reported (fatigue analysis, level ground running strength analysis, downhill walking strength analysis). Safety factors to material yielding are calculated.

4.1 Quick release mechanism design criteria

In a posterior strut AFO, the strut is securely bolted to the proximal and distal AFO sections, requiring tools and time to change struts. To make the device portable, the QRM must be operated by hand without tools and be integrated into the AFO components. Users are expected to swap struts within 30 seconds (Table 4-1).

The QRAFO must work robustly under the design criteria weight, without failure. The QRM should function appropriately for at least three years under normal activities without material failure or mechanism problems.

Table 4-1 QRM design criteria

Item	Criteria
Connection with orthosis	Affixed
QRM width	Equal or less than the strut width
Release method	Tool-free
Steps to swap strut	Maximum 4 steps
Time to swap strut	Maximum 30 seconds
Weight	Maximum 50 grams

The QRM will be located between the energy return strut and orthosis. A compact size not exceeding the strut width would reduce the chance of the QRM being damaged during use or the user being hurt by contact with the QRM. Therefore, the QRM width should not exceed the strut width.

QRM weight is important for user acceptance and reducing the energy burden for "carrying the AFO" during the day. Therefore, the QRM should be as light as possible while not sacrificing strength. The QRM design target is less than 50 grams.

4.2 Quick release mechanism model

4.2.1 Quarter turn fastener model

Figure 4-1 shows a quarter-turn fastener (QTF) quick-release mechanism model concept. Two quarter-turn keys, affixed on the strut, are used to lock the entire mechanism. One weight-bearing pin bears the body-weight load. Corresponding receptacles for the quarter-turn keys can be affixed on an anchor, which is molded into the orthosis.

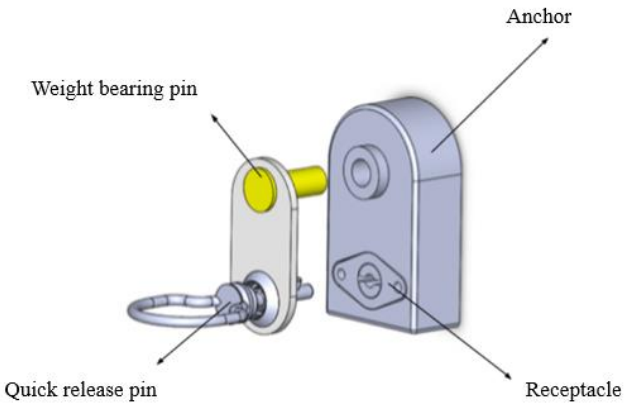

Figure 4-1 Quarter turn fastener mechanism.

The QRM locks by aligning the strut and orthosis, pushing the male assembly into the female assembly, and turning the quarter-turn key.

4.2.2 Sliding locking model

A sliding locking mechanism (SLM, Figure 4-2) uses a latch pin as the locking mechanism. The latch pin is attached to a trapezoidal male carrier and fits another female anchor with a trapezoidal groove. The carrier side surface and the inner anchor surface are in contact and prevent

sagittal plane motion. During gait, sagittal plane forces are taken by the carrier and anchor, thereby reducing force on the latch pin. Three holes on the anchor allow the user to adjust AFO cuff height. The pin only takes shear load when multidirectional forces and moments exist. A spring between the carrier and latch pin pulls the latch into the anchor hole. The spring ends affix to the carrier and latch pin. The anchor is attached on the orthosis posterior surface and the carrier is affixed on the posterior strut. The lock procedures are: 1) align the strut and orthosis, 2) slide the carrier on the strut into the anchor on the orthosis, 3) align hole and latch pin and release the latch.

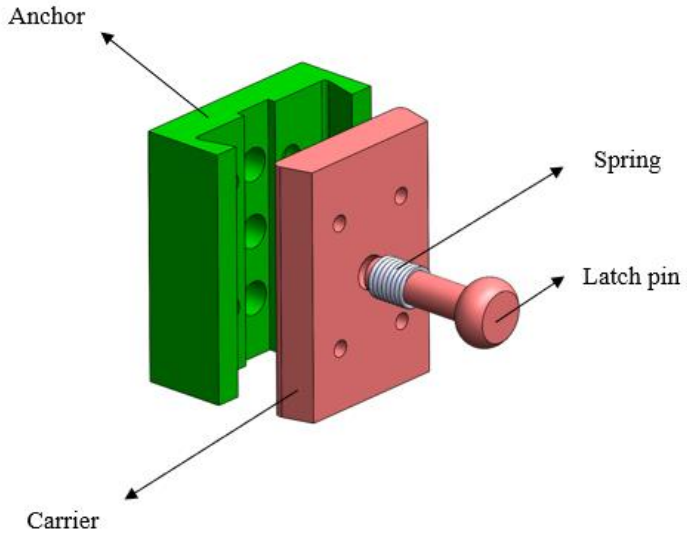

Figure 4-2 Sliding lock mechanism

4.2.3 Quarter-turn cam lock model

Figure 4-3 shows the quarter-turn cam lock (QTCL) model. One anchor with a pin hole will be on the orthosis. Other components will attach to the strut. The locking mechanism will be limited in a carrier affixed to the strut. The locking mechanism includes the octagon cam, pin board, and spring. The pushing pin board lies on the carrier's bearing so that motion is limited to one direction. The cam pushes the pin board and locks the anchor with the carrier by turning the cam 90 degrees. The spring pushes the pin board back to the unlock position by turning the cam for another 90 degrees (Figure 4-4). The flat surface stabilizes the mechanism by providing a large contact area between pin board and cam.

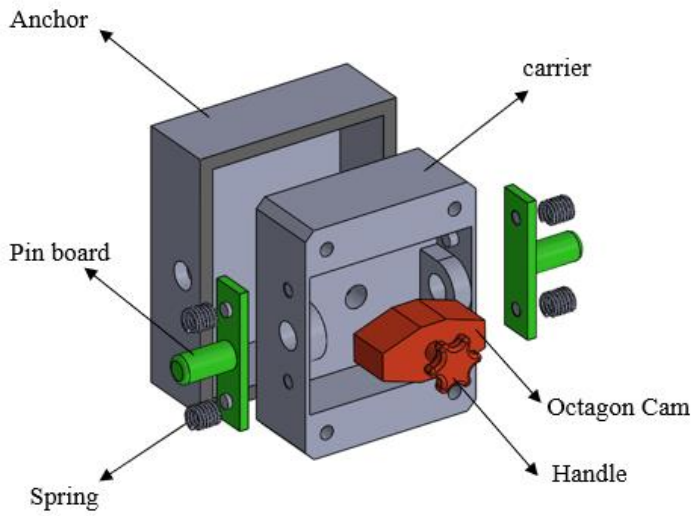

Figure 4-3 Quarter-turn cam lock model.

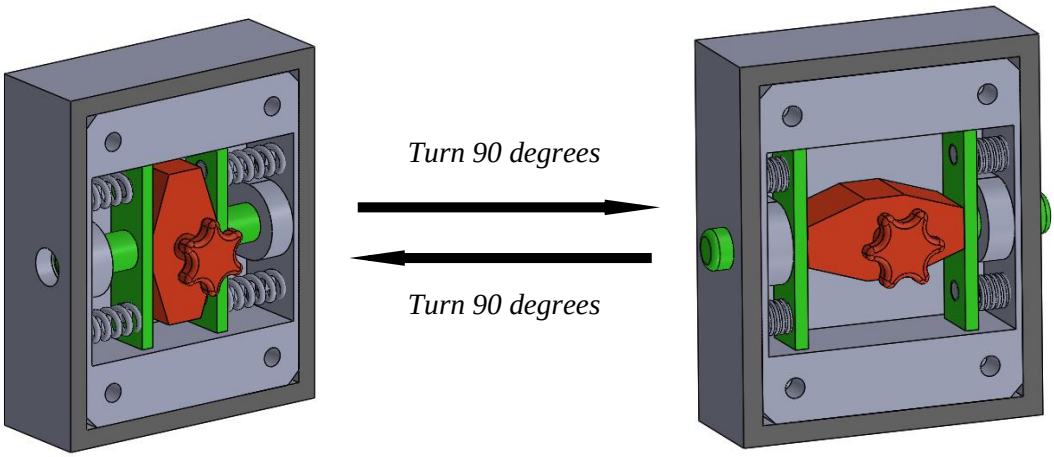

Figure 4-4 Quarter-turn cam lock locking operation by turning the octagon cam

Users lock the mechanism by aligning the strut and orthosis, pushing the male assembly into the female assembly, and turning the cam.

4.2.4 Concept Evaluation

The quarter-turn fastener model is less bulky since its male components can be affixed directed on the strut. The turning operation is limited by the turning directions, with the user turning the key only in one direction to lock the QRM. This mechanism takes two steps to lock and requires sagittal plane alignment. The number of component types added to the orthosis is four. For

manufacturing, the anchor needs one machine tool, either CNC milling machine or regular milling machine. The pin, quarter-turn key, and receptacle can be purchased.

Security is highlighted with the sliding lock mechanism. The trapezoidal shape fit between the carrier and anchor reduced the risk of being pulling out. The locking operation is one step, as simple as releasing the latch pin. However, two alignment processes are required before releasing the latch pin, including aligning the carrier with the anchor groove and aligning the latch pin with the anchor holes. The number of component types is four, and two of these can be purchased off-the-shelf. The carrier and anchor need to be machined with a milling machine. More manufacturing time should be spent on the slope surface of the carrier and anchor.

The quarter-turn cam lock model can be easily operated by turning 90 degrees in either direction. This mechanism takes two steps to lock and needs frontal plane alignment. The number of component types added to the orthosis is five, while the handle and springs can be purchased. For manufacturing, the pin board and carrier need more than two machine tools, such as mill machine and lathe, to manufacture the QRM.

Table 4-2, the quarter-turn fastener model has more positive aspects than the other two models. Therefore, the QR AFO was prototyped using the quarter-turn fastener mechanism.

Table 4-2 Concept selection criteria

	Locking Effort			
	Steps to lock	**Lock motion limits**	**Steps to Align**	**Alignment planes**
QTF	2	Turn one direction	1	Sagittal
SLM	3	None	2	Frontal and Sagittal
QTCL	2	None	1	Sagittal
Best Models	QTF, QTCL	SLM, QTCL	QTF, QTCL	QTF, QTCL
	Efforts on acquiring parts			
	# part types	**# purchasable parts**	**# machine jobs**	**# machine tools**
QTF	4	3	1	1
SLM	4	2	2	1
QTCL	6	2	4	2
Best Models	QTF, SLM	QTF	QTF	QTF, SLM
	Bulkiness and Security			
	Required carriers or anchors		**Motion prevention**	
QTF	Only the anchor		Motion between pin and anchor	
SLM	Both carriers and anchors		Motion between carrier and anchor	
QTCL	Both carriers and anchors		Motion between carrier and anchor	
Best Models	QTF		SLM, QTCL	

4.3 QRAFO modeling

4.3.1 QRAFO CAD prototype

The QRAFO model was divided into three sections: top orthosis, carbon fibre strut system, and bottom orthosis (Figure 4-5). The quick-release mechanism consisted of a quick-release key, receptacle, and titanium pin. The receptacle was epoxied with the anchor and they were affixed in the orthosis and covered with carbon fibre. The quick-release components (quarter turn fastener, receptacle) were purchased from Skybolt Aeromotive Corporation (ZG2600R2, SK213-2, Cloc®, Appendix B). The quarter-turn fastener and the titanium pin (Ti-pin) were epoxied with the strut. Grade 5 titanium (Ti-6V-4Al) was selected to improve strength. An immobilization pin (IM-pin) located between the quarter-turn fastener and the Ti-pin prevented unnecessary plantar plane motion. An adjustment panel was located between the strut and quarter-turn fastener.

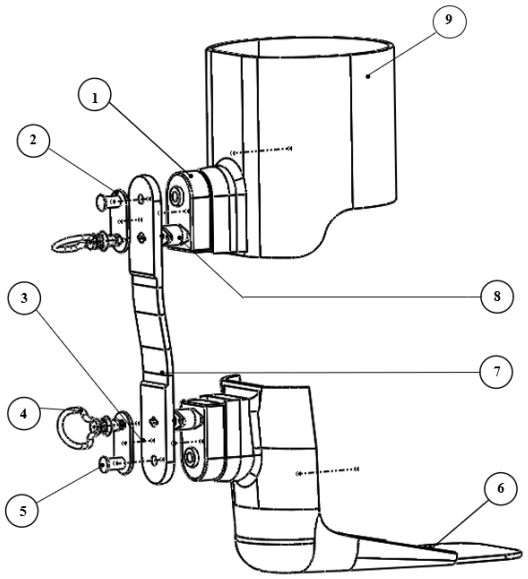

Part Number	Name
1	Anchor
2	Thickness compensation plate
3	Immobilization pin
4	Quick-release key
5	Titanium pin
6	Orthosis sole
7	Energy return strut
8	Cam lock receptacle
9	Orthosis cuff

Figure 4-5 Quick-release AFO prototype and its components in exploded view

4.3.2 Quick release mechanism

The quick-release mechanism consists of a Ti-pin, quick release key, receptacle, anchor, IM-pin, and an adjustment panel (Figure 4-6). The receptacle was epoxied with the anchor, which was molded into the orthosis. The Ti-pin took the role of weight-bearing, by contacting the anchor first when load was applied, to protect the quarter-turn fastener. Machined grade 5 Ti-pins that had enough strength to withstand landing impact were purchased. Pin length was longer than the quarter-turn fastener's stud length so that pin alignment assists stud alignment. Using only one receptacle makes the quick-release mechanism more compact. An adjustment panel between the fastener and strut minimized axial motion between the strut and quarter-turn fastener. Clearance between the quick release key and receptacle caused rotation around the Ti-pin, between the strut and orthosis. The IM-pin was crafted to prevent this rotation.

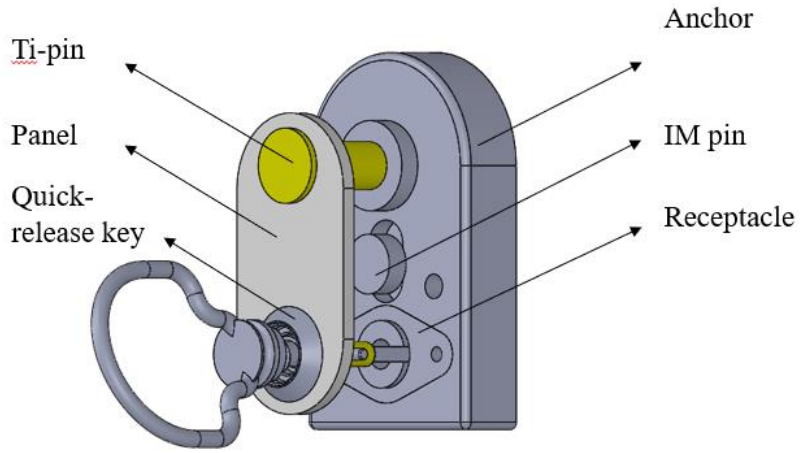

Figure 4-6 Quick release mechanism

The quarter-turn fastener consisted of the stud, sleeve, and spring. A foldable bail handle that can fold into a flat position was selected (Figure 4-7). A spring between the sleeve and key shaped metal provided push out force that helped the key remain stable when locked with the receptacle. The quick-release key had a foldable bail so that the key was able to remain low profile. The immobilization pin was constructed from a cylindrical and another rectangular part. The cylindrical end was epoxied with the strut and the rectangular end fit the anchor slot.

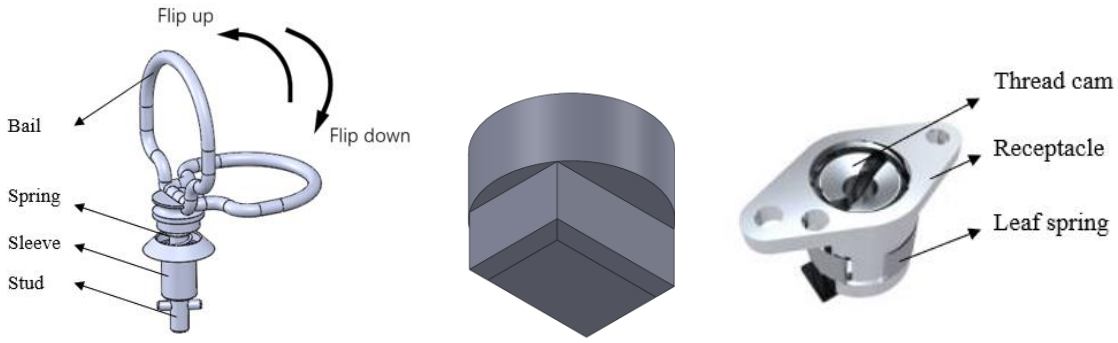

Figure 4-7 Foldable bail design quick release key (left), immobilization pin (middle), and quick release receptacle (right)

The hollowed anchor design (Figure 4-8) reduced weight while guaranteeing strength. The extruded cylinder and Ti-pin were clearance fit, thereby enabling smooth lock and unlock movement. The diamond shape groove fit the receptacle. The receptacle and anchor were press-fit and epoxied to ensure the receptacle was fixed securely. A slot at anchor center fit the IM pin.

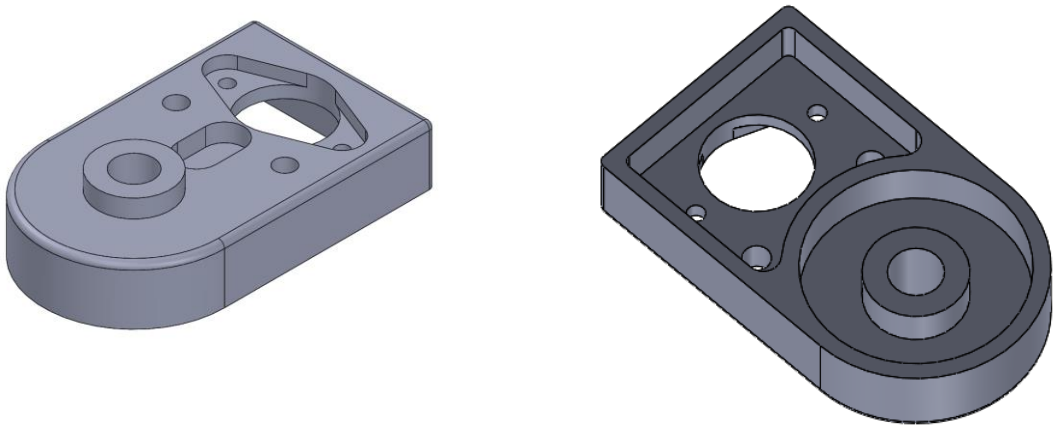

Figure 4-8 Anchor isometric view from top (left); Anchor isometric view from bottom (right)

The receptacle was adjustable, with a thread cam shape screw (Figure 4-8). The thread cam could change position and then maintain the position with a leaf spring. The quick-release key travelled through the groove, inside the screw, and locked. The adjustable design provided a larger range of clamped panel thicknesses. The strut swapping steps were: 1) align the pin to the anchor, on orthosis calf and foot shells; 2) push the strut into the orthosis; 3) turn quarter-turn fastener to lock the device. Model materials are listed in Table 4-3.

Table 4-3 Parts, materials, and sources for the quick release mechanism

Part	Material	Source
Anchor	Aluminum 6061	Machined from raw material
Pin	Titanium Alloy Ti-6Al-4V	Allied Titanium Inc.
Quarter turn fastener	Aluminum 6061	Skybolt Aeromotive Corp.
Receptacle	Aluminum 6061	Skybolt Aeromotive Corp.
IM-pin	Acetal	Machined from raw material

4.4 FEA mechanical analysis

Mechanical analysis is important as a preliminary determination of appropriate material and geometric decisions. Material failure of the QRM or AFO can hurt the end user. For example, if the energy return strut breaks or the quick release key detaches during movement, improper foot-ground contact that could produce a stumble or fall. QRM failure or deformation could disable the quick release mechanism, lead to the strut being stuck in the AFO or the user not being able to reattach the strut into the AFO, leaving the person to unsafely walk without their AFO.

The AFO design in this thesis followed regular clinical practice for PDEAFO. Therefore, the AFO strength is not discussed in the thesis and FEA modelling focussed on QRM components.

4.4.1 Assumptions

QRM design assumptions are:

- QRM can be attached to an offloading orthosis. Eighty-percent weight offloading from the foot was considered in the design.
- QRM can withstand a person walking on a 20-degree ramp without material failure.
- QRM can withstand loads when running at 5 m/s without material failure.
- User inertia when moving was not considered.
- Friction between the quick release male and female components was not considered.
- The device will be used mostly in moderate climate conditions.
- Adhesive material around the QRM will not fail.
- Orthosis and strut deformations were negligible for calculation.
- For calculations, 10 ms^{-2} was considered as gravity acceleration.

4.4.2 Level ground fatigue analysis formulation

QRAFO was designed for long periods of daily use. Fatigue failure occurs when an object is subjected to time-variable loading. Commonly, the fatigue strength is well below the ultimate static strength [62], [63]. Fatigue strength when the specimen reaches infinite life length is called the endurance limit. While the stated endurance limit of grade 5 titanium is 510 MPa, the actual endurance limit is affected by component loading conditions. Modifying factors are defined and used to account for long-period repeated loading using Marin equation [63]

$$k = k_a k_b k_c k_d k_e k_f \tag{4-1}$$

where k is the modifying factor, affected by six different subfactors: surface modification (k_a), size (k_b), loading (k_c), temperature (k_d), reliability (k_e), and miscellaneous effect (k_f).

The actual endurance limit modified by Marin factors is

$$S_e = kS'_e \tag{4-2}$$

where S_e denotes the actual endurance limit and S'_e is the ideal endurance limit.

Factors were estimated for pre-design phase. The surface modification factor is affected by the quality of the part surface. Lipson and Noll presented an experience equation for the surface modification factor [63]

$$k_a = a(S_{ut})^b \tag{4-3}$$

where S_{ut} is the ultimate tensile strength, and a and b are regression factors.

The size effect should be considered and expressed by the size factor. Mischke et al. [64] derived equations for size factor based on 133 sets of data points. The small circular rod equation is

$$k_b = \left(\frac{d}{7.62}\right)^{-0.107} = 1.24d^{-0.107}\ 2.79 \le d \le 51\ mm \tag{4-4}$$

where d is the diameter of the Titanium pin and k_b is the size factor.

Fatigue tests illustrate the difference between three types of loading [65]. This difference can be compensated by a loading factor, k_c, which is given by

$$k_c = \begin{cases} 1 & bending \\ 0.85 & axial\ Load \\ 0.59 & torsion \end{cases} \tag{4-5}$$

Temperature affects the material properties, becoming a consideration when the temperature is higher than 449°C [62]. The QRAFO is assumed to work at room temperature, for which the temperature factor equals one.

The standard deviation of endurance strength is less than 8 percent. The reliability factor can be written as

$$k_e = 1 - 0.08 z_a \tag{4-6}$$

where z_a is the transformation variate to reliability factor k_e.

The miscellaneous-effect factor is mutually affected by corrosion, electrolytic plating, etc. The QRAFO design did not consider these factors.

Walking generates fluctuating stresses among the QRM component. Walking can be regarded as a cyclic load with the same mathematical patterns such as the mean, amplitude, period length. A modified Goodman equation is introduced to describe the relationship between the mean and load amplitude while the life of the parts is at the boundary of infinity.

$$\frac{\sigma_a}{S_e} + \frac{\sigma_m}{S_{ut}} = 1 \tag{4-7}$$

where σ_a is the amplitude component of fluctuating stress, and σ_m is the midrange component.

Modified Goodman equation determines the actual fatigue safety factor. The safety factor to infinite life is defined and applied to the equation

$$\frac{\sigma_a}{S_e} + \frac{\sigma_m}{S_{ut}} = \frac{1}{n} \tag{4-8}$$

where *n* indicates the safety factor regarding infinite life.

The design was based on calculations with 80% percent body weight offloaded by the AFO cuff. Research found that PTBAFO off-loading effects decreased by time, with body weight offloading decreasing to 54.9% after two weeks and to 43.7% after long term use [66]. The QRAFO design covered more than 90% percent of the body weight range in the USA population [54]. The titanium weight bearing pin strength in the QRAFO design had more than double the strength of the two steel bolts used in the commercially available PDEAFO. Therefore, a desired safety factor of one is sufficient for the analyses in this thesis (i.e., in practice the steel bolts are sufficient to safely secure a strut to an AFO).

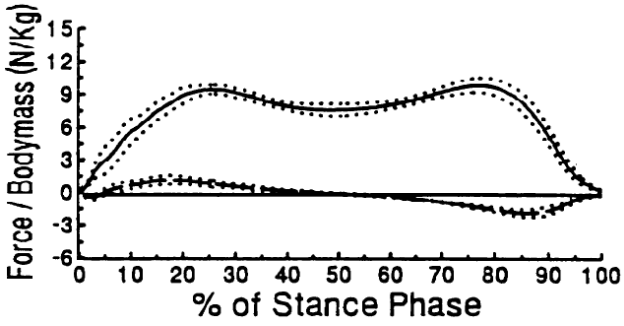

Figure 4-9 Ground reaction forces normalized by body mass for one step while walking on level ground. Normal force, solid line; shear force, dashed line; standard deviations, dotted lines [61].

The maximum ground reaction force during walking on level ground equals bodyweight. (Figure 4-12) [61].

Maximum stress was calculated by SolidWorks simulation (Figure 4-10). Shear force was considered in the simulation. The quick release key and receptacle took no load due to the clearance between these parts. The calculation combines equations (4-2) and (4-8). Since the Modified Goodman safety factor was 5.09, the Ti-pin will not have material failure caused by fatigue.

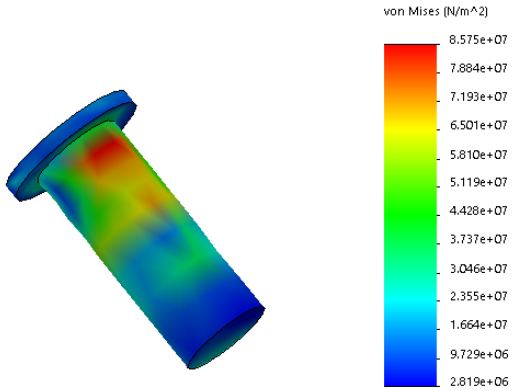

Figure 4-10 SolidWorks simulation result of Ti-pin under maximum walking load

Aluminum alloys usually do not exhibit a distinct endurance limit. The experimental fatigue strength of aluminum for 10^7 cycles is approximately 117 MPa [67]. Considering the stress concentration factor, the anchor simulation is shown in Figure 4-11.

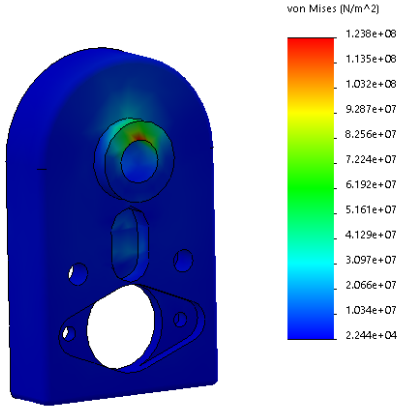

Figure 4-11 Solidworks simulation result of anchor under walking load

The Modified Goodman safety factor is 1.37 for the anchor. Both Ti-pin and anchor show a low chance of failure due to fatigue.

4.4.3 Level ground running load analysis

The QRM must support large impact forces when the user performs intense activities. Failure to absorb impact on the components can transfer the energy to the user and cause injury. Two intense conditions were applied to the design, level running and walking on a 20-degree descending hill.

Kenneth et. al. [57] found that the maximum ground reaction force during running (5 m/s) can reach three times body weight (Figure 4-12). Maximum load occurred around mid-stance, where the ankle maintains a neutral position. Therefore, the force exerted on the QRM was hypothetically along the strut's long axis. Shear force was considered between the QRM and orthosis when running on level ground.

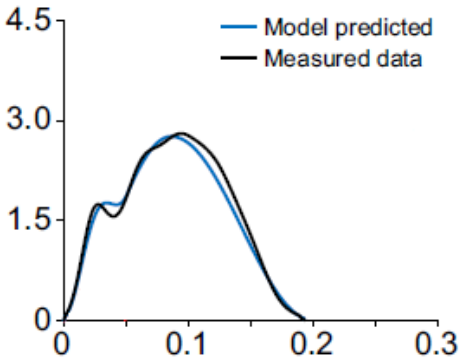

Figure 4-12 Vertical ground reaction force-time waveform predicted by model (5 m/s running) [57].

Stress on the Ti-pin can be expressed as,

$$\tau = \frac{V}{A} \tag{4-9}$$

where τ is the shear stress in the pin, V is the shear force applied on the pin, and A refers to the cross-section area.

The selected grade 5 titanium has a yielding strength of 880 MPa. Therefore, the pin should not fail. A FEA meshed model was built for the simulation (Figure 4-13). Two rigid fixtures were designed to simulate the QRM assemblage. Uniformly distributed forces were exerted on the end of the flat bar. The shell holding anchor was set as a global fixture. The flat bar's side surface could only deform in the x or z directions. Y-direction motion was restricted to prevent numerical error accumulation in the y direction. The clearance interfaces, such as interface between Ti-pin and anchor, interface between flat bar and shell, and interface between flat bar and anchor, were contact surfaces with no penetration conditions. Other interfaces were bonded.

To simulate the real situation, a nonlinear solver was used to allow contact conditions to change due the Ti-pin's slide behavior. Von Mises stress was calculated among all mesh elements. Figure 4-14 presents the stress distribution through Ti-pin and anchor, with maximum stress noted.

Compared with the Ti-pin and anchor yielding strength (880 MPa and 270 MPa), yielding safety factors were 5.5 for Ti-pin and 1.07 for the anchor.

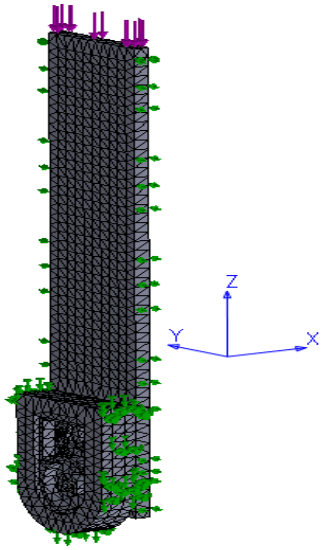

Figure 4-13 Load and fixture position on meshed QRM equivalent to running load

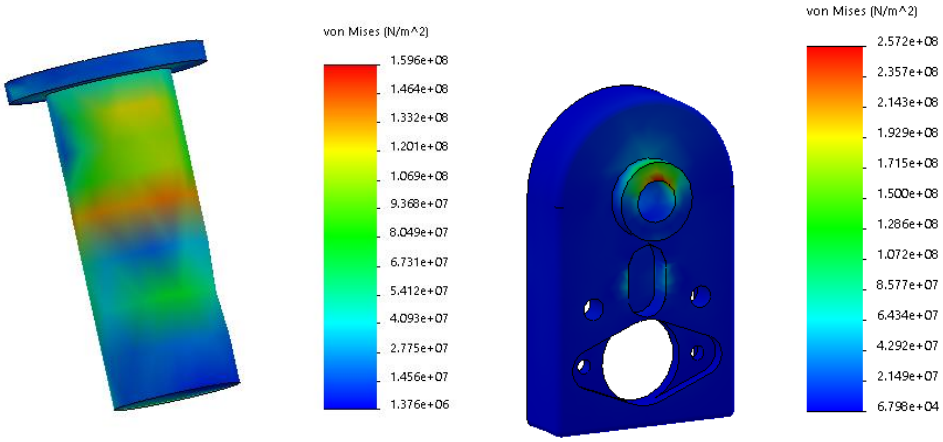

Figure 4-14 Solidworks simulation of Ti-pin and anchor under running load

4.4.4 Downhill walking load analysis

Biomechanics research suggests that peak vertical ground reaction force while descending a 20-degree ramp is 12 times the body mass (Figure 4-15) [61], producing 1440 N vertical load on the foot for a 120 kg person.

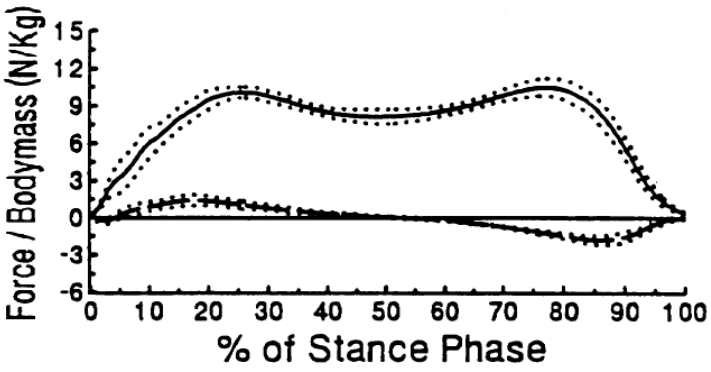

Figure 4-15 Ground reaction forces normalized by body mass for one step while descending a 20-degree ramp. Normal force, solid line; shear force, dashed line; standard deviations, dotted lines [61].

The strut free-body diagram for a person walking on a 20-degree hill is shown in Figure 4-16. By assuming body weight is exerted on the quick release joint, the free body diagram when walking on a 20-degree hill is shown in Figure 4-16. Forces exerting on two different sole locations produced a moment on the quick release joint, which was compensated by a reaction moment from quick release mechanism.

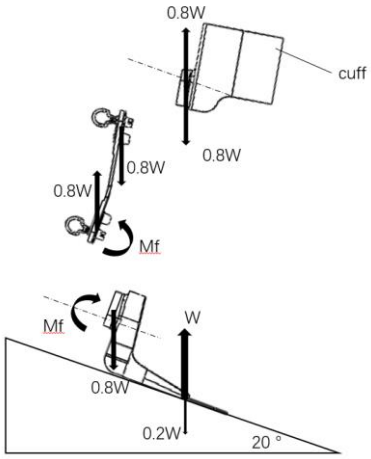

Figure 4-16 Free body diagram of strut during downhill walking, where W is user body weight, M_f is the reaction moment. 80% body weight is exerted on cuff and 20% body weight on the sole.

A bending moment was exerted on the QRM due to the inclined position. Equation (4-10) calculated the moment on the QRM.

$$M_f = 0.8WL\sin(20^o) \tag{4-10}$$

where L indicates the strut length, W is the transferred weight to the orthosis, and M_f denotes the bending moment generated on the QRM.

The distance between two Ti-pins on the strut accounted for the moment. The moment on a 250 mm long strut was 86.7 Nm with 220 mm lever length. The force component along the strut was

1080 N and the transverse force perpendicular to the strut was 394 N. The force along the strut produced a shear stress on the Ti pin. The force perpendicular to the strut produced a bending moment on the QRM, and also a pulling force on the quick release key.

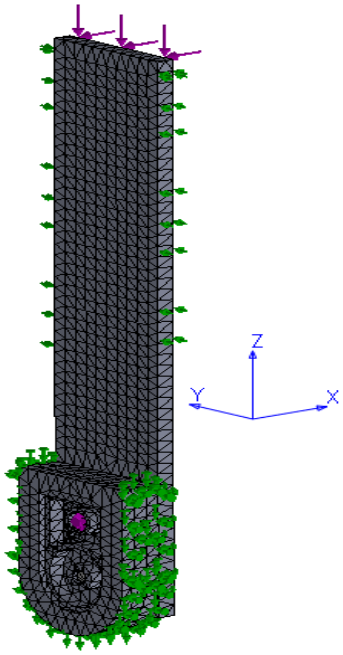

Figure 4-17 Load and fixture position on meshed QRM with downhill walking impact load

A FEA model was built with a rigid flat bar and rigid shell (Figure 4-17). The distance between the flat bar's upper bound and the Ti-pin hole was 220 mm. A 1080 N sagittal plane load was exerted uniformly on the flat bar's upper surface. To generate a moment on the QRM, a 394 N force in the negative *x* direction was applied on the edge of the flat bar's upper surface. The rigid shell was fixed globally. Since the load should cause deformation only in the sagittal plane, flat bar frontal motion was prohibited so that numerical errors would not diverge. The mesh size of the quick release components (quick release key, receptacle) and other components were controlled separately. Small-value curvature-based mesh was applied to the quick release components due to its complex shape, aiming to provide precise results.

A nonlinear solver was used to calculate Von Mises stress among all mesh elements. Figure 4-18 presents the stress distribution through the Ti-pin and anchor, with maximum stress noted.

Downhill walking results were different from the running load results. Stress on the Ti-pin shifted to the front under bending moment. Larger stress on the Ti-pin also occurred. The quick release key stud and receptacle took less stress during bending. Overall, the components were more vulnerable when an inclined load was applied. Safety factors are listed in Table 4-4.

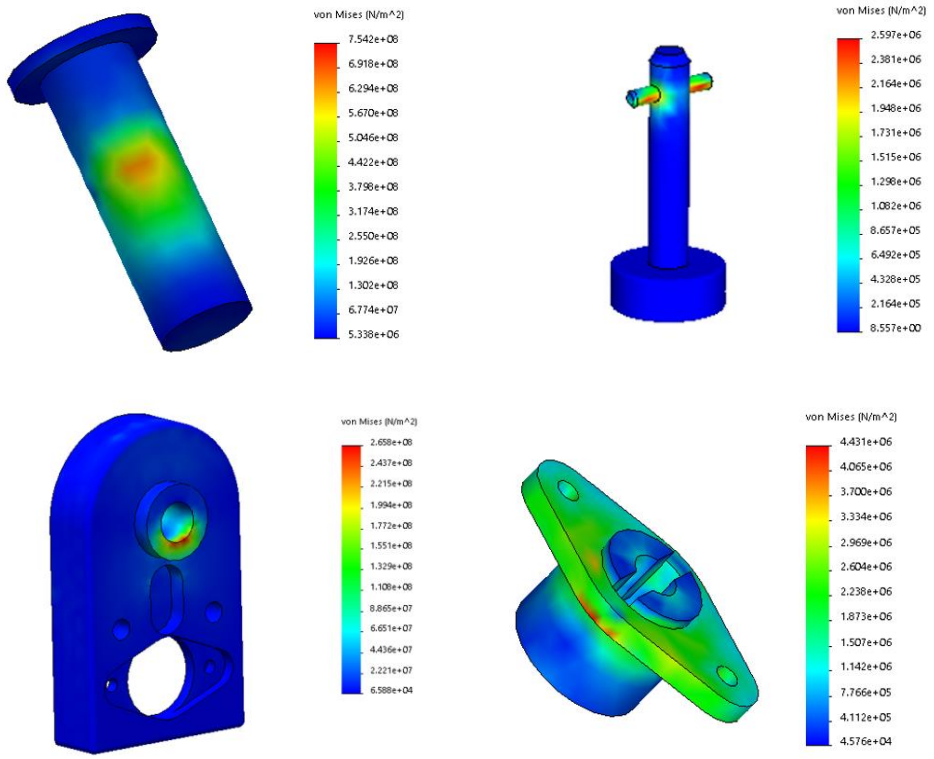

Figure 4-18 Solidworks simulation of Ti-pin and anchor under downhill walking load

Table 4-4 Maximum stress and safety factors of the QRM parts

Quick-release Parts	Running		Downhill Walking	
	Max. Stress (MPa)	Safety Factor	Max. Stress (MPa)	Safety Factor
Ti-pin	159.6	5.51	754	1.17
Anchor	257.2	1.05	266	1.02
QR key			26	10.38
QR receptacle			44	6.14

4.4.5 FEA result analysis on Ti pin

The Ti-pin simulation results showed larger stress for downhill walking compared to running. To verify the relationship, the stress on Ti-pin was estimated. The stress during running is mainly shear stress ((4-11)).

$$\tau = \frac{V}{A} \tag{4-11}$$

Where V is the shear force, A is the area of Ti-pin, and τ is the shearing stress. Since the Area of Ti pin is quadratic with the radius, the transformation of shear stress is expressed as equation (4-12),

$$\tau = \frac{V}{\pi r^2} \tag{4-12}$$

Since the downhill walking load caused a moment on Ti-pin, the stress on Ti-pin is dominated by bending stress shown in (4-13).

$$\sigma = \frac{Mr}{I} \tag{4-13}$$

Where σ is the maximum bending stress under bending moment M, and I is the inertia of Ti-pin. The inertia is quartic with radius, which transforms equation(4-13) to equation(4-14).

$$\sigma = \frac{2M}{\pi r^3} \tag{4-14}$$

The denominator of bending stress is smaller than that of shearing. Therefore, the Ti-pin is more vulnerable with the downhill walking load compared to the running load.

4.5 Summary

The simulation results show that the QRM is safe for level walking, running, and downhill walking scenarios. The most vulnerable condition was the user walking on a 20-degree descending hill. Inferring from this result, downhill and stair walking would have higher chances of device failure due to the bending moments. These results can have biases due to assumptions and numerical errors. Mechanical tests should be performed under appropriate loading conditions to ensure that the device can withstand the loads transferred to the device from running or downhill walking.

Chapter 5: Mechanical Evaluation

This chapter presents mechanical testing methodologies and results from the quick release mechanism (QRM). Two tests evaluated device performance with running load and downhill walking load. Section 5.1 and 5.2 present the test protocol and the results. Section 5.3 discusses the test results and presents a series of failure analyses.

5.1 Testing methodologies

Mechanical tests were performed with running (2880 N) and downhill walking (1080 N vertical, 394 N horizontal, 86.7 N/m bending moment) loads. The QRM components should have no failure, such as plastic deformation or surface damage, under these loads. Connections between components should remain in the original state after testing.

5.1.1 Running load testing protocol

High strength steel (Grade 4140, cold roll, annealed) was selected as the jig material that functioned as orthosis and strut. The quick release stud and receptacle, anchor, and Ti-pin components were separated into two groups: male parts attached to the "strut" and female parts affixed on the "orthosis". The "orthosis" was machined and fitted to the anchor and receptacle. The "strut" was connected with the "orthosis" by the QRM (Figure 5-1).

The tests were performed using an electromechanical testing machine (4482, InstronR, Norwood, MA) with a 10 kN static load cell (10 N resolution, ISO-376, InstonR, Norwood, MA [68]). Two fixture positions were available on the machine. The top fixture had a cylindrical shape with an iron plate beneath. The iron plate's horizontal surface provided force along the vertical axis. The bottom fixture had a jaw shape to clamp the specimen.

The load cell provided 2880 N maximum force at a constant speed of 1 mm/min. The steel strut was clamped on the testing machine. The load cell initial position was manually set to approximately one millimeter from the iron shell. A smartphone was fixed on a tripod and video recorded the trials. When the force sensed by the load cell reached 2880 N or the displacement reached 10 mm, the load cell terminated action and returned to origin position. Ten trials were collected and analyzed.

(a)

(b)

(c)

Figure 5-1 (a) Testing setup for downhill walking impact test; (b) anchor fitting in "orthosis" with press fit; (c) quick release key and Ti-pin epoxied with "strut"

The Instron machine used Bluehill software to create the test method and record data at 10 Hz. Load cell displacement and force data were saved in comma-separated values (CSV) format. Video data were collected from the smartphone and saved as MOV format. After testing, the force-displacement relation was explored by analysing the slope of the curve. Besides, quick release component dimensions were measured by a calliper with 0.01 mm resolution (Accusize Industrial Tools, AB11-1106) before and after testing to determine surface damage between Ti pin and aluminum anchor.

5.1.2 Downhill walking load testing protocol

The downhill walking load test was similar to the running load test since QRM components were affixed on the same "orthosis" and "strut" and the same testing machine and load cell were used. However, the top fixture was replaced with a 20-degree triangle hot rolled steel part that provided force in two directions. The fixture on the bottom (jaw shaped clamp) secured the specimen.

The load cell provided 1080 N maximum force at a constant speed of 1 mm/min. The steel strut was clamped on the testing machine (Figure 5-2). The load cell's initial position was manually set to one millimeter away from the iron shell. A smartphone was fixed on a tripod and recorded the procedures. Note that the machine can only detect the vertical force and displacement. The load cell would terminate action and return to origin position if the vertical load reached 1080 N. Ten trials were collected and analyzed.

Figure 5-2 Testing setup for downhill walking test

5.1.3 Data processing

The load cell started at a different location during each trial. Therefore, the "touching point" of the data (Figure 5-3), where the load cell touched the specimen, was identified so that the measured displacement would be equivalent to specimen deformation along the strut. The maximum measured force before the load cell touching the specimen was below 10 N. The maximum value was tracked from zero displacement until a 5-sample string larger than 10 N occurred. The first sample subtracting from this 5-sample string was set as the touching point. Data before the touching point was discarded.

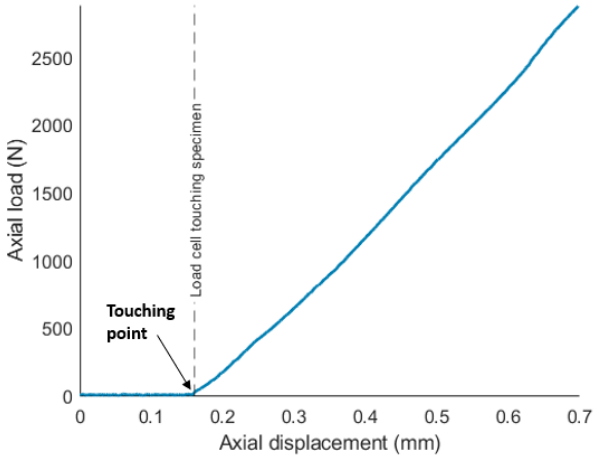

Figure 5-3 Running load test (trial 1) unprocessed data, showing force-displacement relationship

Data collected from the sensor contained noise from the displacement sensor, load cell force sensor, material surface roughness, etc. Raw data were normalized to 500 points using spline interpolation, and the spectrum of data was normalized from 0 to 1. Force data were filtered using a 4th order Butterworth filter with normalized cut off frequency of 0.10 πrad/sample (Figure 5-4) to keep the major part of the spectrum.

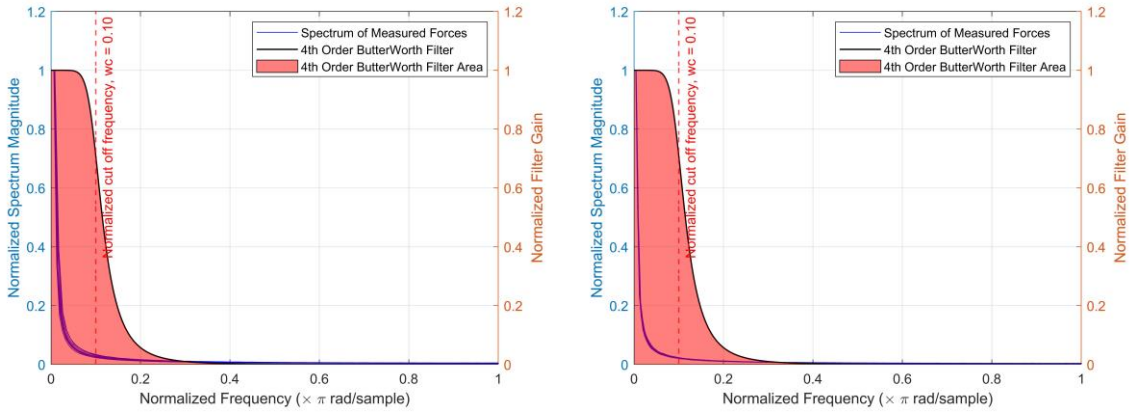

Figure 5-4 Spectrum of measured forces and the Butterworth filter with running load (left) and downhill walking load (right)

After removing noise, the force-displacement curves were analysed. Pearson correlation coefficients (PCC) for force-displacement curves and slope-displacement relations were calculated to assess trial similarity.

5.1.4 Dimension evaluation

Any displacement caused by deformation and surface damage can lead to the dimension change after tests. Measurable component dimension changes included Ti-pin diameter, Ti-pin length, and anchor pin hole diameter. A calliper with 0.01 mm resolution (Accusize Industrial Tools, AB11-1106) was used. Twenty measurements were made at different locations on each measured component, before testing, after running load test, and after downhill walking load test. Mean and standard deviation were calculated after each test.

5.2 Mechanical evaluation results

5.2.1 Running load

Load cell forces monotonically increased in relation to material deformation (Figure 5-5). The slope of the curve did not decrease, indicating that the material did not reach the yielding point where plastic deformation occurs.

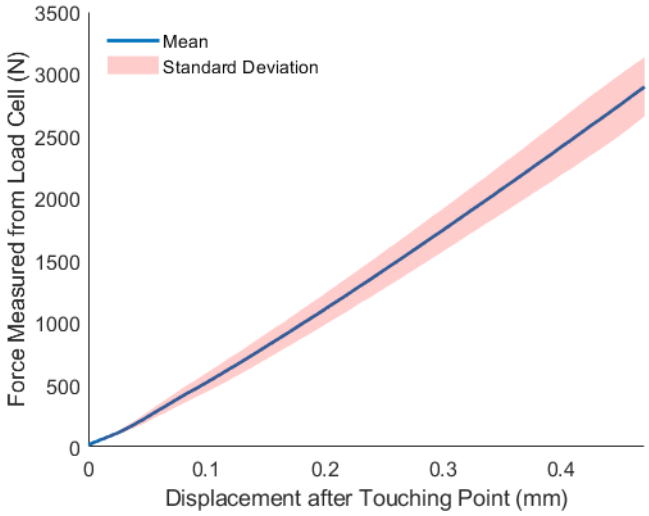

Figure 5-5 Force-displacement curve plotted from the running load data

PCC between each force-displacement curve was larger than 0.99. PCC close to 1 indicates that datasets are highly similar. Therefore, the running load tests were repeatable.

5.2.2 Downhill walking load

Load cell force monotonically increased with respect to displacement (Figure 5-6); therefore, the material did not reach the yielding point where plastic deformation occurs. This evidence showed that components were in their elastic region when the downhill walking load was applied.

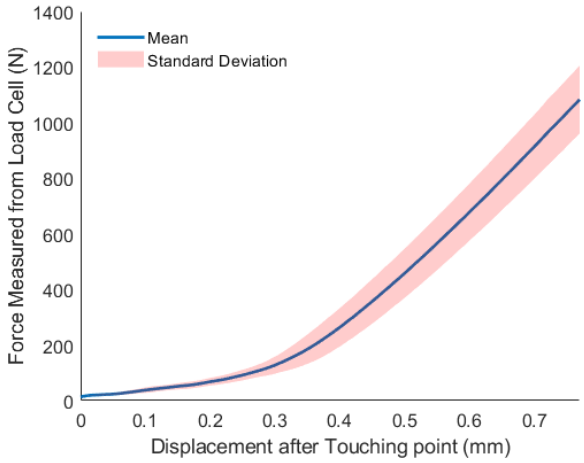

Figure 5-6 Force-displacement curve from 20-degree downhill walking load test

PCC between each force-displacement curve was larger than 0.99. Therefore, the downhill walking load tests were repeatable.

5.2.3 Dimension measurements

Table 5-1 shows mean and standard deviation of the measured dimensions. The mean of the Ti-pin diameter, Ti-pin length, and anchor hole diameter were within 0.02 mm of their original dimensions. Since the caliper resolution was 0.01 mm and small human error may have occurred for caliper placement, these results are within expected measurement error. Therefore, testing did not produce permanent dimension change on Ti pin, anchor hole. Standard deviations were smaller than 0.02 mm, so measurements along one surface were consistent. Therefore, surfaces were not damaged due to running and downhill walking loads. Overall, no failure evidence was found from the testing results.

Table 5-1 Means and standard deviations (mm) of the original dimensions and dimensions after running load and downhill walking load tests

	Before Testing	**Running Load**	**Downhill Load**
Ti-pin diameter (mm)	6.29 (0.01)	6.29 (0.02)	6.28 (0.01)
Ti-pin length (mm)	21.10 (0.01)	21.11 (0.01)	21.09 (0.01)
Anchor hole diameter (mm)	6.37 (0.01)	6.38 (0.01)	6.38 (0.01)

5.3 Summary

The mechanical tests evaluated QRM performance on three aspects: plastic deformation, surface damage, and trial repeatability. The monotonically increasing force-displacement curves showed that QRM components were in the elastic deformation region within the maximum running or downhill walking load. Pearson correlation coefficients between trials were close to 1, reflecting high similarity between trials from the same test. Therefore, the running tests and downhill walking tests were repeatable. The similar measurement results showed that surface damage did not occur between Ti pin and anchor. The QRM was verified to have no failures under running and downhill walking loads.

Chapter 6: Quick Release Evaluation

This chapter evaluates QRAFO swapping performance, which is defined as:

- The time to take off and reattach the quick release strut (criterion = less than 30 seconds)
- Strut swapping time using QRAFO is less than the time to swap struts using PDEAFO

Strut swapping time is an important parameter for QRAFO function that affects end-user acceptance. The time required to remove and reattach a strut was compared between a test AFO with the QRM and a test AFO with the strut screwed into the AFO (i.e., same attachment method as PDEAFO). This test received ethics approval from University of Ottawa (Appendix E).

6.1 Test AFO

Two AFO were designed and 3D printed for the quick release timing tests (Figure 6-1). Both orthoses had identical components (strut, cuff, foot plate) and were manufactured in PLA using an Ultimaker 2+ printer. One orthosis was configured as a QRAFO, with a QRM bonded to a PLA strut (250 mm length, 6.35 mm thickness). The second AFO secured a PLA strut to the cuff and foot plate with 1/4-20 machine screws and 3D printed anchor (screw anchor system). The two AFOs were modeled in SolidWorks (Appendix A, Figure A-0-3 to Figure A-0-5). The participant wore the 3D printed AFO on their right foot within their shoe during all tests.

Figure 6-1 3D printed AFO with quick release mechanism (left) and screw-anchor mechanism (right)

The cuff was secure on the leg by a strap with a loop-and-hook end (Velcro®). Two parts formed the cuff: the cuff body and snap shell. The cuff body accommodated the strap and fit the users calf, and the snap shell press fit the cuff body and fixed the anchor and receptacle to the cuff (Figure 6-2). The shell inner dimension equaled the anchor dimension (30×50×9.5 mm). The snap shell was secured on the cuff body with silicone. The quick release key and Ti pin were affixed on the strut using instant adhesive (Gorilla Glue®). At the back of foot plate, an identical snap shell was affixed on the foot plate with the anchor and receptacle wrapped. The foot plate was secured on the foot by a shoe.

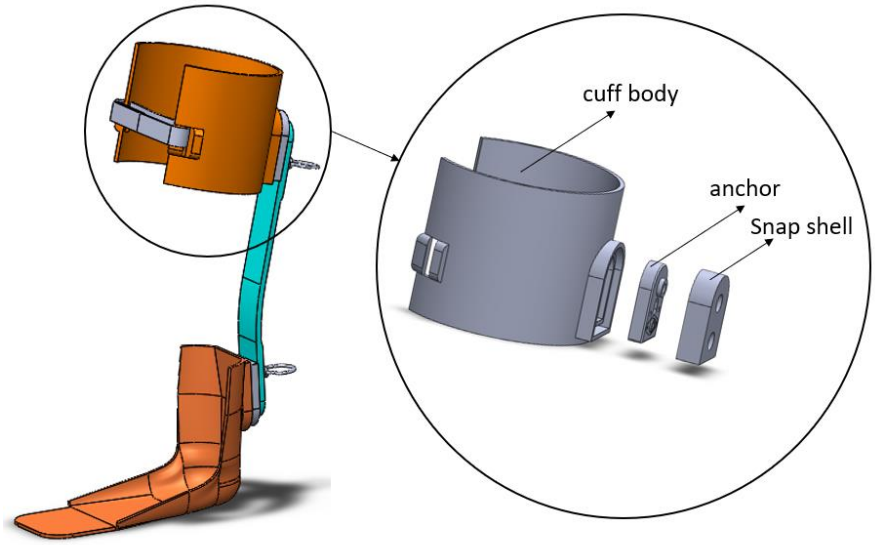

Figure 6-2 3D printing AFO and cuff components

6.2 Methods

To record trials, a GoPro was held by the investigator to collect video data at 30 fps, thereby enabling movement timing and qualitative performance evaluation.

Four able bodied participants were recruited (3 males, 1 female). While sitting, the participant removed the strut, waited for 2 to 4 seconds, and then reattached the strut. This trial was repeated 10 times.

The time for strut removal and strut attaching was calculated by determining the start and end time for each movement from the video. For QRAFO testing, strut removal started when the participant's hand touched the QRM and ended when all strut components (strut, quick release key and Ti pin) were not contacting the QRAFO. Strut attaching started when one of the strut components touched the AFO and ended when the hand was not touching the QRM (Figure 6-3). For the screw-anchor connection AFO, removal started when a screwdriver touched the AFO and ended

when strut components (strut and screw) were not contacting the AFO. Attaching started when the strut components touched the AFO and ended when the screwdriver was not contacting the AFO. Strut swap time is the sum of removal and attaching times.

Figure 6-3 An example of the starting of strut removing (left) and starting strut attaching (right)

Video Editor software from Microsoft Inc was used to identify the starting and ending frames. The video segments located between starting frames and ending frames were cropped and exported as mp4 files. Eighty trials were exported into 160 videos (80 attaching and 80 removing, with QRM and screw anchor mechanism). The video segments durations were then extracted using MATLAB.

6.3 Results

The mean average swap time of 4 participants with QRM was 25.01 ± 3.66 seconds. Figure 6-4 shows that average swap time with QRM for all participants was within 30 seconds. On average, participants spent 17.63 ± 3.61 seconds for strut attaching and 7.38 ± 1.79 seconds on strut removing. Strut alignment to the orthosis was the primary reason why attaching a strut took more time than removing the strut. The best swap time was 13.83 ± 3.08 seconds, with best attaching time of 8.81 ± 2.17 seconds and best removing time of 4.20 ± 2.31 seconds.

As a comparison, the mean average swap time of 4 participants with screw anchor mechanism was 60.48 ± 10.88 seconds, 142% larger than swap with QRM. Figure 6-5 shows that average swap time with the screw anchor mechanism of all participants was more than 30 seconds. Participants spent 39.94 ± 10.42 seconds averagely on strut attaching, 127% larger than attaching with QRM, and 20.55 ± 2.25 seconds averagely on strut removal, 178% larger than removal with

QRM. The best swap time with screw anchor mechanism was 38.71 ± 3.43 seconds, larger than the 30 seconds criterion.

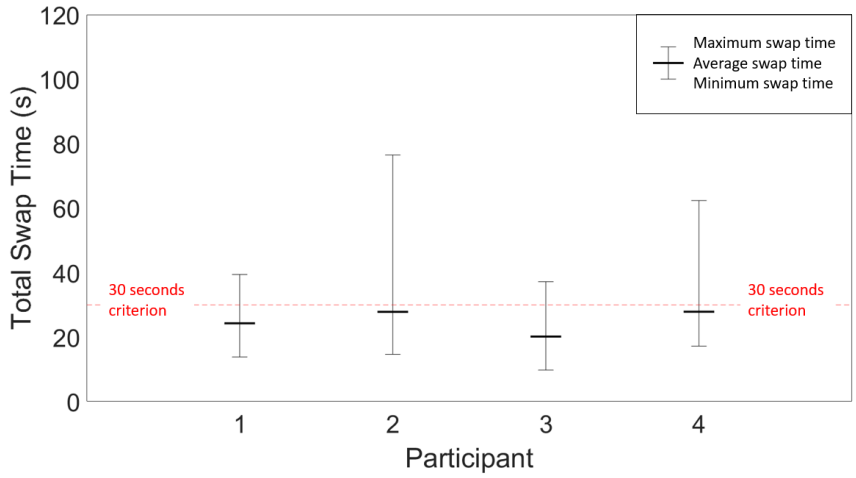

Figure 6-4 Range and mean of total swap time of QRM

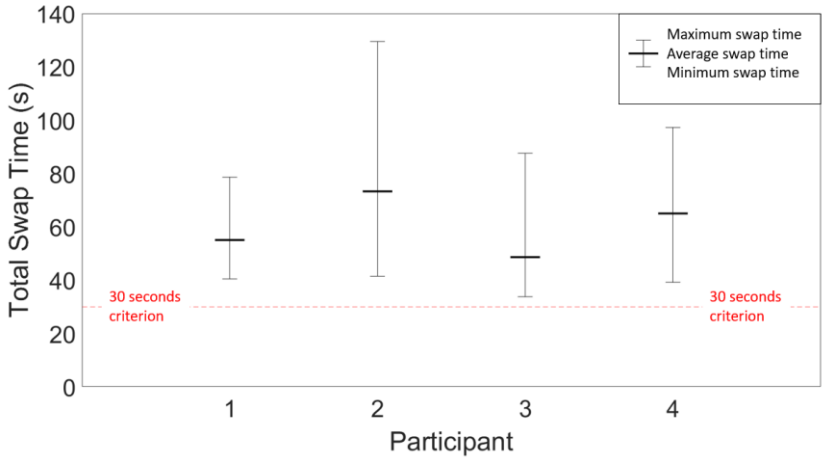

Figure 6-5 Range and mean of total swap time of screw anchor mechanism

6.4 Strut swap behaviour test

Section 6.3 revealed large differences between maximum swap time and minimum swap time. Participant learning the method to swap strut was the reason for the differences. A strut swap behaviour test studied the learning effect of strut swap. The behaviour test was performed by a graduate student (25 years, male).

6.4.1 Methods

To record trials, a smartphone was affixed on a tripod to collect video data at 30 fps, thereby enabling movement timing and qualitative performance evaluation.

The test AFOs were described in Section 6.1. While sitting, the participant removed the strut, waited for 2 to 4 seconds, and then reattached the strut. This trial was repeated 10 times. After at least 2 hours, an additional 10 removal and reattachments trials were completed. This was repeated until a total of 50 trials were collected. This protocol was completed for both QRM and screw-anchor mechanism.

Video Editor software from Microsoft Inc was used to segment the videos. Fifty trials were exported into 100 videos (50 attaching and 50 releasing). The video segments durations were then extracted using MATLAB.

6.4.2 Results

The average time to swap struts with the QRM was 13.85 ± 6.52 seconds and the screw-anchor was 58.41 ± 11.16 seconds. As the participant learned how to best swap the strut, the best swap time improved from maximum 35.95 seconds to 6.81 seconds. Figure 6-6 shows the learning effect since strut swapping time decreased over the first 30 trials. The first ten strut swaps averaged 23.97 seconds and the last ten swaps averaged 8.92 seconds. Standard deviation also improved, with a standard deviation of the first ten trials of 5.22 seconds and the last ten trials of 1.43 seconds.

Less time was needed to remove the strut than attach the strut. Over the first ten trials, the average time to attach the strut was 19.70 ± 5.08 seconds, while the last ten trials were 6.24 ± 0.90 seconds (68.3% decrease). The average time to remove the strut, over the first ten trials, was 4.27 ± 0.68 seconds and the last ten trials was 2.68 ± 0.82 seconds (37.2% decrease). QRM swapping time was less than the 30-second design criteria.

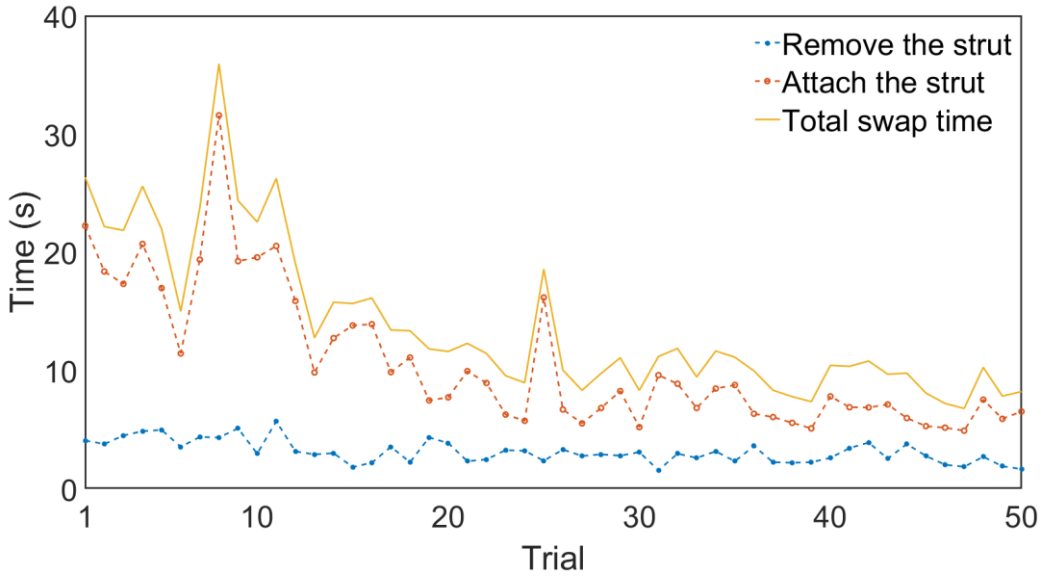

Figure 6-6 Time to swap strut with QRM

In comparison, the screw-anchor mechanism averaged 58.41 ± 11.16 seconds to swap (Figure 6-7). A milder learning effect was seen. The average time to swap the strut for the first ten trials was 73.39 ± 7.98 seconds, including a mean attaching time of 50.37 ± 4.71 seconds and a mean removing time of 23.01 ± 6.23 seconds. The average time to swap the strut for the last ten trials was 47.85 seconds, with a mean attaching time of 33.07 seconds and a mean removing time of 14.78 seconds. The time decrease in total swap time between the first ten trials and last ten trials was 34.8%, including a 34.3% decrease in attaching and 35.8% decrease in removing. Standard deviations were also larger than the QRM results. The standard deviation of the first ten trials was 7.98 seconds, and that of the last ten trials was 3.74 seconds. Therefore, more time is required to swap struts when using an AFO with the screw-anchor mechanism, and the 30-second swapping criterion was not achieved.

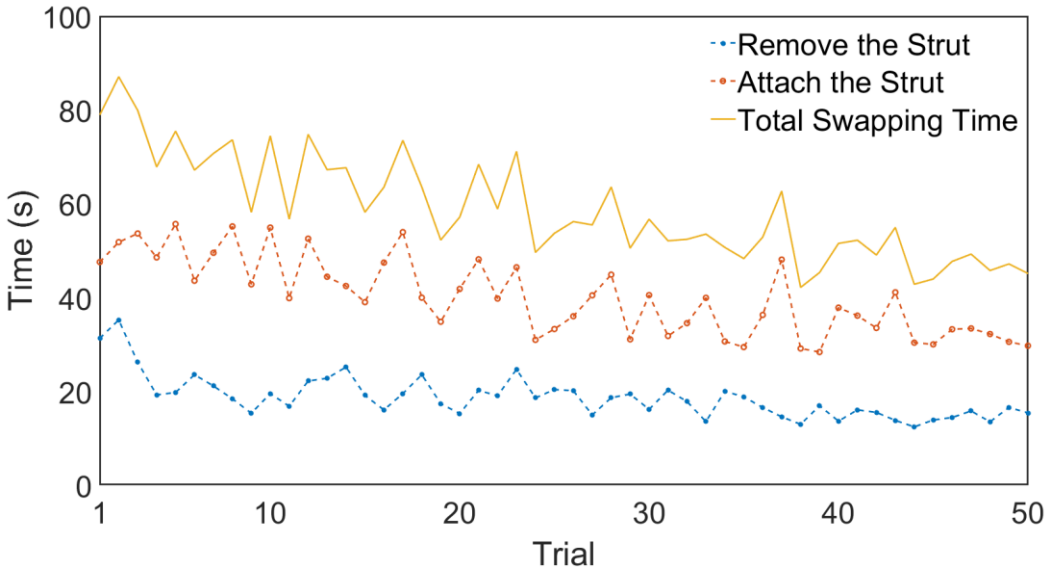

Figure 6-7 Time to swap strut with screw anchor mechanism

The difference between maximum swap time and minimum swap time for the last 10 trials was distinctively decreased. For strut swap with QRM, maximum swap time for last 10 trials was 10.82 seconds, while the minimum swap time was 6.81 seconds. For strut swap with screw anchor mechanism, maximum swap time for last 10 trials was 55.00 seconds, while the minimum swap time was 42.88 seconds.

Table 6-1 lists the time to swap strut by mechanism test for each group and movement.

Table 6-1 Average time for removal and attachment for QRM and screw-anchor, in groups of 10 trials (standard deviation in brackets)

	QRM	**Screw-anchor**
Strut attaching (1-10)	19.70 (5.08)	50.37 (4.71)
Strut attaching (41-50)	6.24 (0.90)	33.07 (3.48)
Strut removing (1-10)	4.27 (0.68)	23.01 (6.23)
Strut removing (41-50)	2.68 (0.82)	14.78 (1.33)
Strut swap (1-10)	23.97 (5.22)	73.39 (7.98)
Strut swap (41-50)	8.92 (1.43)	47.85 (3.74)

6.5 Summary

This section evaluated QRM performance on swap time. The average swap time of QRM on the 3D printed QRAFO 24.08 seconds, which satisfies the 30-second target in the design criteria. Furthermore, the average swap time after practising was 8.92 seconds, which outperformed the 30-second design criterion. The participant spent 81.36% less time on QRM than the screw-anchor mechanism used in PEDAFO in the last ten trials. Considering that the QRM can be swapped without tools, the QRM outperformed screw-anchor mechanism on strut swap.

Chapter 7: QRAFO Prototype

This chapter presents the QRAFO fabrication processes and displays the QRAFO prototype. The QRAFO was fabricated by an orthotist and orthotic technician at The Ottawa Hospital Rehabilitation Center Prosthetic and Orthotic Department.

7.1 Carbon fibre lamination

As described in section 4.3, the QRM was designed to be bonded with QRAFO components. The anchors and receptacles were molded in the QRAFO cuff and foot plate, and the quick release keys, Ti pins, and immobilization pins were bonded on the strut. Carbon fibre fabric was laminated over the anchor and molded anchor.

7.1.1 Lamination components

Figure 7-1 shows the quick release mechanism components. QRM materials are listed in section 4.3.2. During lamination, the receptacle thread cam (Figure 7-1) was taken out of the receptacle. The receptacle was then affixed on the anchor by metal epoxy adhesive (+PLUSeries®). The strength of epoxy adhesive ranges from 5.17 to 97 MPa [69]. Despite low strength, the epoxy takes mild resistance force between receptacle and anchor while user accidentally pulling or pushing the strut. Two locating holes (6-32 thread) were machined in the anchor to guide and position the strut dummy plates during lamination (Figure 7-2).

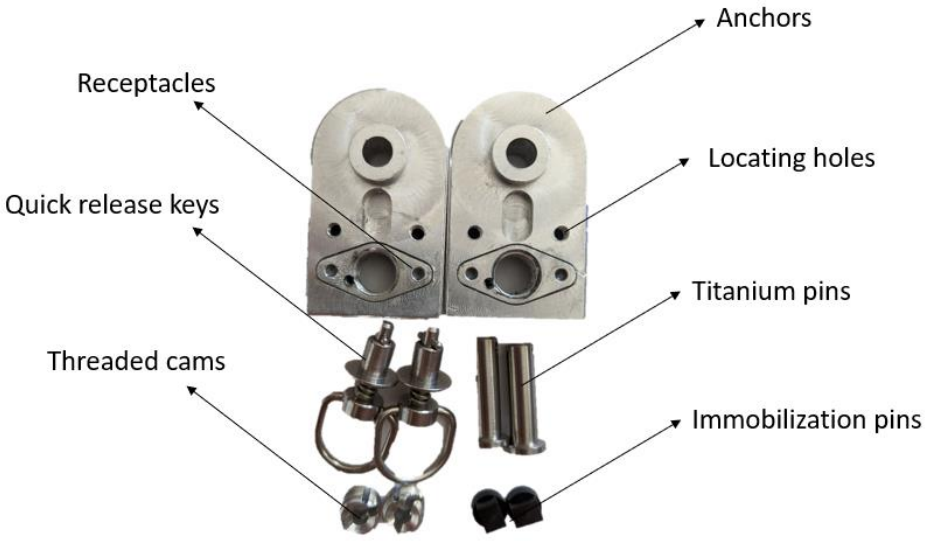

Figure 7-1 Quick release components

Lamination tools (Figure 7-2) were designed and manufactured to assist carbon fibre fabric lamination over anchors. Table 7-1 shows the lamination tools specifications, including, names, materials, manufacturing methods, and functions.

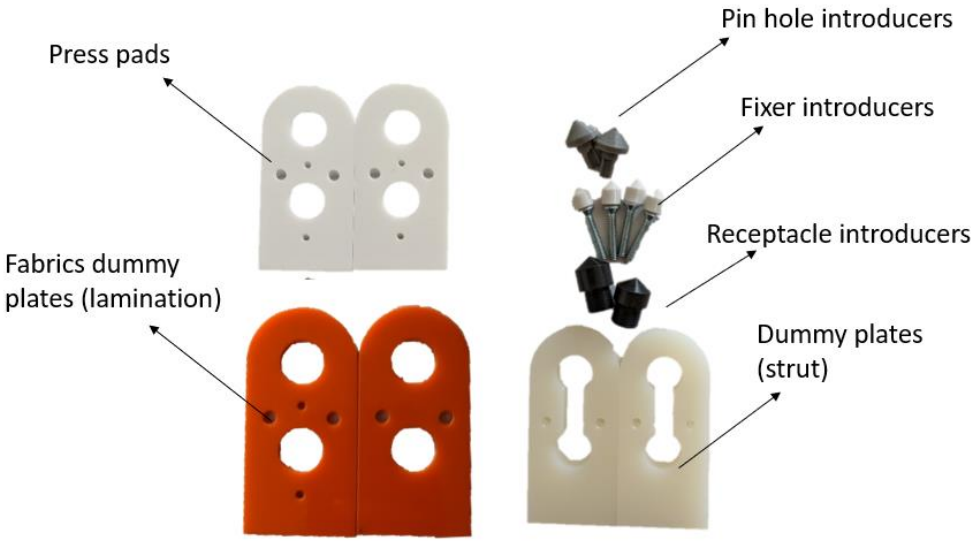

Figure 7-2 Lamination tools

Table 7-1 Lamination tools specifications

Tool	Material	Manufactured/Purchased	Functions during Lamination
Press pads	Acrylic	Laser-cut using Epilog Laser Helix 24×18 60 W	While carbon fibre fabric was laminated over the anchor, the press pads pressed the fabrics to pack the fabrics tightly.
Pin hole introducer	PLA	Printed by Ultim aker 2+	Before lamination, the pin hole introducer was placed in the anchor pin hole. Fabrics were laminated over anchor through the pin hole introducer, thereby leaving the pin hole uncovered.
Fixer introducer	Steel screws and PLA	6-32 x 7/8 screws were purchased. Introducers were printed by Ultimaker 2+. Two parts were bonded by silicone	Before lamination, the fixer introducer was threaded in the anchor's locating hole. Fabrics were laminated over anchor through the fixer introducer, thereby leaving the locating hole uncovered. After lamination, the dummy plate (strut) was placed over

			the carbon fibre fabrics, and the fixer introducer was threaded in anchor threaded hole to lock the dummy plates with fabrics.
Receptacle introducer	Acetal	Machined from raw material	Before lamination, the receptacle introducer was threaded in the receptacle. Fabrics were laminated over anchor through the receptacle introducer, thereby leaving the receptacle thread hole uncovered.
Dummy plate (lamination)	Acrylic	Laser-cut using Epilog Laser Helix 24×18 60 W	The lamination dummy plate was located between anchor and strut before lamination. The dummy plate had the same thickness as lamination.
Dummy plate (strut)	Nylon	Machined from raw material	The strut dummy plate was the dummy for the strut end. During lamination, the strut dummy plate was placed over the lamination. In addition, the strut dummy plate kept the lamination surface smooth and flat during the curing of resin.

7.1.2 Strut modification

The QRAFO prototype utilized the PDEAFO strut. The orthotist chose the strut length for the user. Quick release key, Ti-pin, and immobilization pin were bonded to the strut. Without changing the original strut hole diameter, the orthotist used a rotatory tool to machine posts on the inner hole. In the middle, between pin hole and keyhole, a 5/16-1/8 sink hole was milled to fit the immobilization pin (Figure 7-3).

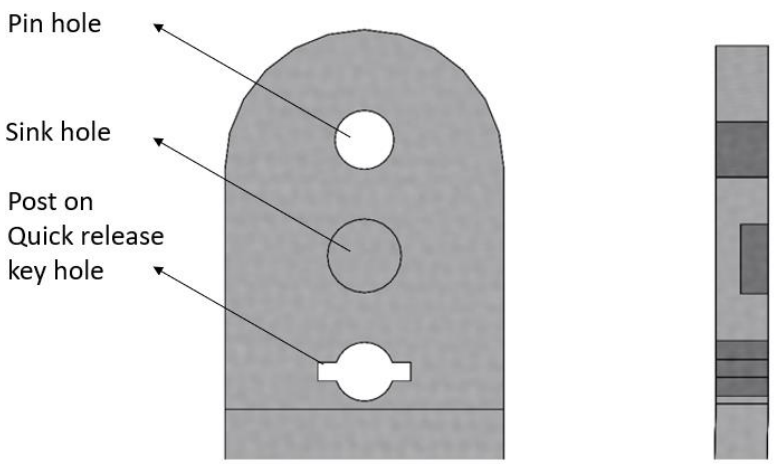

Figure 7-3 Strut modification (transparent view) ; front view (left); side view (right)

7.1.3 Lamination procedures

1. Bond quick release key, Ti-pin, and immobilization pin with strut.
2. Stack lamination dummy plates on anchors. Then place the assemble strut from step 1 over dummy plates (Figure 7-4). Turn quick release key to lock anchors and lamination dummy plates with strut.

Figure 7-4 Assembly of QRM, dummy plates and strut

3. Once assembled, bond the anchor using adhesive (+PLUSeries® Composite) on a target leg cast model along posterior sagittal plane of the leg model.
4. After the adhesive cured (1 minute), remove the strut, dummy plate, quick release key, threaded cam and Ti pin.
5. Insert Introducers into anchor pin holes, receptacle threads, and anchor locating holes (Figure 7-5).
6. Fill the anchor slot with silicone.

7. During lamination, the carbon fibre fabrics laminate through introducers, thereby leave the cavities unlaminated. The cone shape on the top of introducers aided carbon fibre fabrics laminating over the anchor through Introducer.

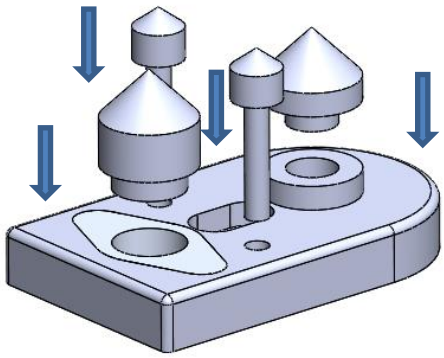

Figure 7-5 Introducers to cover anchor cavities (except slot in the middle).

8. Laminate two layers of 45-degree carbon fibre fabric (12 K weight) over the anchor and then three 0/90 orientation carbon fibre fabric (12 K weight) layers as reinforcement (Figure 7-6). Spray adhesive over the anchor surface and between each carbon fibre fabric layers during lamination.

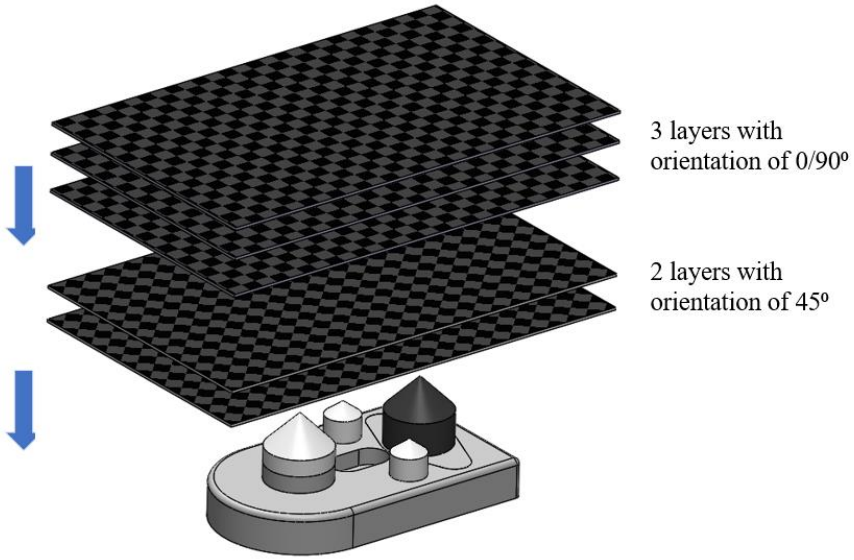

Figure 7-6 Carbon fibre fabric laminating over the anchor

9. Remove fixer introducers.
10. Use press pad to press the lamination and pack the lamination tighter (Figure 7-7). Remove the press pad after this step.

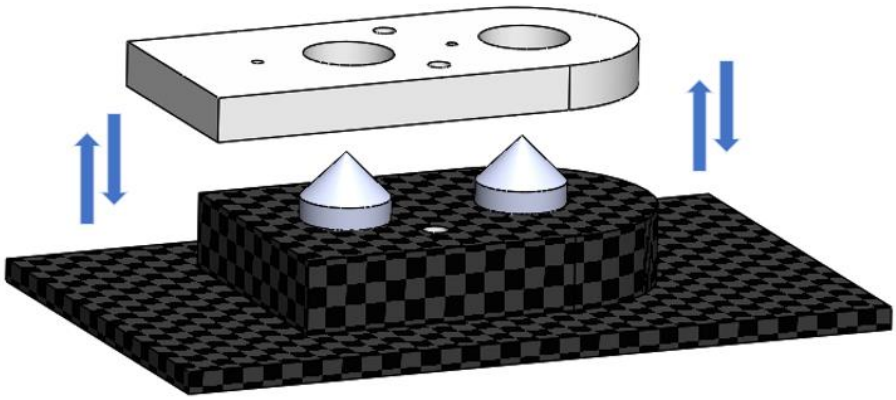

Figure 7-7 Lamination packed by press pad

11. Place strut dummy plates over the anchors and introducers.
12. Tighten strut dummy plates on lamination with fixer introducers (Figure 7-8). Dummy plates keep the lamination surface flat and smooth as the resin hardens.
13. Laminate the orthosis body over the QRM lamination layup.
14. Seal and fill the entire lamination with resin.

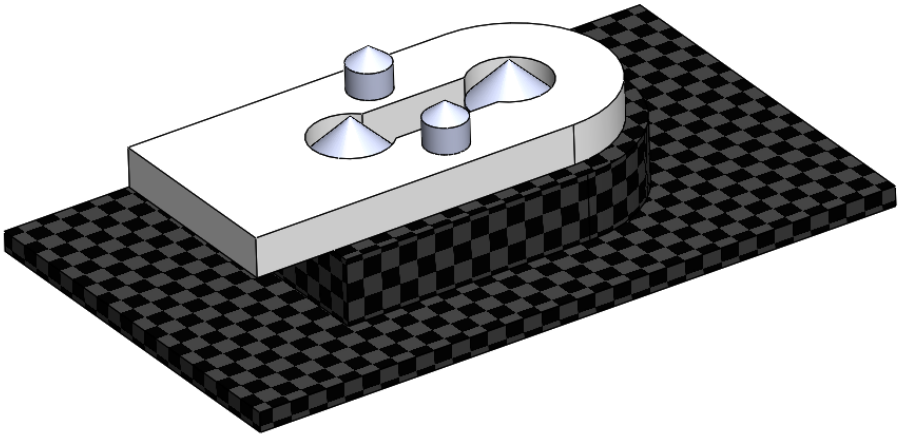

Figure 7-8 Dummy plate pressed lamination, fixed by fixer introducer

15. After the resin hardened, remove the introducers and machine a slot on the QRAFO through dummy plate slot.
16. Remove strut dummy plate.
17. Assemble the orthosis with strut and quick release male components.

7.2 QRAFO Prototype

Figure 7-9 shows the QRAFO prototype. The prototype was fabricated in the Prosthetic and Orthotic Department in Ottawa Hospital Rehabilitation Centre. The prototype was fitted to the orthotist who fabricated this QRAFO. The QRAFO prototype was configured with PDE strut (250 mm) and QRM. The Ti pin, quick release key and immobilization pin were bonded with the strut with glue (+PLUSeries®). A loop-and-hoop strap was mounted on the cuff to secure the cuff on the calf. The QRAFO weighed 1112 grams and the QRM weighed 30 grams. The prototype validated the fabrication process of QRAFO.

Figure 7-9 QRAFO prototype

Chapter 8: Conclusions and Future Work

8.1 Conclusions and limitations

In this thesis, the quick release strut swapping system of a novel quick-release ankle-foot orthosis was designed and evaluated to address current PDEAFO limitations. The quick-release mechanism allows individuals with dorsiflexor/plantarflexor weakness to tune their AFO to their daily activities; such as, driving, walking, downhill walking, and running. This design was low profile so that the orthosis will fit beneath normal clothing. The weight added on the strut is minimal, which motivates users to carry extra struts with different stiffness levels during the day. The QRAFO was developed in consultation with the staff of the Ottawa Hospital Rehabilitation Centre.

The quick-release mechanism meets the design criteria. The design was lightweight and compact, which would allow the user to wear the orthosis beneath standard fitting clothing. The quick-release mechanism components were mostly off-the-shelf, which lowers the device cost. Table 8-1 displays the design criteria and criteria achievement summary.

Mechanical testing revealed that the QRM could bear running and downhill walking loads for a 120 kg person, with no failure from material or connection. Force-displacement curve analysis revealed that QRM materials remained in their elastic region under the maximum target loads. The ten trials showed high repeatability, indicating that the connection was not failing (slipping, dislocating, etc.) under running and downhill walking loads. Titanium did not to harm the aluminum anchor's surface, inferred from low dimension variation between trials.

QRM functional tests demonstrated that the user could swap a strut within 30 seconds. After learning, a user can swap struts in approximately 10 seconds, which outperforms our design criteria. As the participant practiced the swapping movement, swap strut time decreased, and with a smaller time variance.

While the QRAFO met the design requirements for quick release function and strength, the tests were preliminary for developing a general use device. Mechanical testing proved that the quick release mechanism had sufficient strength to support loads from intense activities, such as running and downhill walking, under ideal situations (i.e., occasional intense activities, ideal road and climate conditions). Further research is needed to verify fatigue performance for long duration intense use, such as highly active users and athletes. Fatigue testing with higher loads can determine whether the current material and design has sufficient support.

The climate and road condition criterion are assumed to be moderate. Under extreme cold weather, the high thermal conductivity of aluminum alloy can be cold to the touch when swapping struts. Due to the high tolerance of the Ti-pin and anchor, small particles such as sand, that stay

inside the anchor can require more push and pull force while swapping struts and may damage the anchor hole inner surface with prolonged wear. The issue can also occur for muddy road since the mud can stay in the anchor hole, thereby leading to the difficulty while swapping struts.

Though functional testing verified QRM function, more evaluations are needed to determine whether the device would motivate the user to swap the strut in their everyday life. A future testing protocol with AFO users is required to confirm the perceived usefulness and satisfaction on strut swapping.

Table 8-1 QRAFO design criteria and achievement list

Evaluation items	**Design criteria**	**Outcome**	**Summary**
AFO weight	<1500 grams	1112 grams	Achieved
QRM weight	<50 grams	30 grams	Achieved
Strength	Not breaking during a 120 kg person running or downhill walking, considering 80% cuff off-loading maximum	Mechanical tests on running load and downhill walking load showed no failure	Achieved
Peak joint moment	38.4 Nm for 120 kg person	QRM joint did not fail under 86.7 Nm in downhill walking test	Achieved
ROM	-15-20 degree	Free ankle motion when strut removed	Achieved from design
Device life	Normal walking with 10^7 cycles	Anchor design has a safety factor of 1.37, Ti pin has a safety factor of 5.09	Achieved from simulation
Swapping time	Less than 30 seconds	Approximately 10 seconds after learning	Achieved

8.2 Future work

8.2.1 Mechanical strength for highly active users

While the quick release ankle-foot orthosis is promising, improvements can be made in the future. Simulation of the anchor component revealed that the stress distributed on downhill walking was close to the strength margin. If the user performs downhill walking or running daily, the anchor may fail by fatigue due to long term usage. Therefore, the actual life could be shorter than expected. To not exceed the weight design criteria, high strength aluminum, such as aluminum 2024, may be considered as an improved version.

Mechanical testing proved that the quick release mechanism had enough strength to support intense activities like running and downhill walking. However, for highly active users who use this device mostly associate with intense activities (e.g., soldiers on back to duty training, athletics using the AFO as running support), the anchor could have a risk of fatigue failure. A future mechanical testing protocol should consider long term intense activities.

8.2.2 QRAFO strut fabrication

In this thesis, a PDEAFO strut was modified to incorporate the QRM. However, machining carbon fibre can decrease product strength due to carbon fibre damage. Karataş et. al concluded machined carbon fibre reinforced polymer generally encounters fatigue strength lackness and composite delamination [70]. Stated in Section 7.1.1, the epoxy connection strength between the Ti-pin, quick release key, and strut is less than a laminated carbon fibre connection, therefore the prototype epoxy bonding could lead to failure from impacts or when accidents occur (user falling, etc.). Therefore, in practice, the QRM components should be laminated into the carbon fiber strut during manufacturing, thereby providing a quick swap strut that requires no extra machining and with securely integrated components.

8.2.3 Further QRAFO functional tests

As mentioned in section 8.1, more biomechanical testing should be performed to determine whether the device motivates users to swap struts during the day. The future testing protocol should focus on the users perceived usefulness and satisfaction by qualitive measures. An improved testing protocol should include a large activity range and more participants with lower limb weakness. A potential solution can be designing an activity list (Appendix C) including light activities and intense activities, with a questionnaire (Appendix D) to record QRAFO use satisfaction.

References

[1] "PDE Modular Composite Spring System." http://www.fabtechsystems.com/PDE-Modular-Composite-Spring-System/ (accessed Aug. 20, 2019).

[2] "Ankle," *Wikipedia*. Mar. 04, 2020, Accessed: Mar. 23, 2020. [Online]. Available: https://en.wikipedia.org/w/index.php?title=Ankle&oldid=943919573.

[3] C. L. Brockett and G. J. Chapman, "Biomechanics of the ankle," *Orthop. Trauma*, vol. 30, no. 3, pp. 232–238, Jun. 2016, doi: 10.1016/j.mporth.2016.04.015.

[4] M. W. W. Bs. Ms. M. B. PhD, *An Introduction to Gait Analysis, 4e by Michael W. Whittle BSc MSc MB BS PhD*. Butterworth-Heinemann, 1728.

[5] P. Team, "Phases of the Gait Cycle: Gait Analysis » ProtoKinetics," *ProtoKinetics*, Nov. 28, 2018. https://www.protokinetics.com/2018/11/28/understanding-phases-of-the-gait-cycle/ (accessed Mar. 05, 2019).

[6] M. P. Kadaba, H. K. Ramakrishnan, and M. E. Wootten, "Measurement of lower extremity kinematics during level walking," *J. Orthop. Res.*, vol. 8, no. 3, pp. 383–392, 1990, doi: 10.1002/jor.1100080310.

[7] J. J. Eng and D. A. Winter, "Kinetic analysis of the lower limbs during walking: what information can be gained from a three-dimensional model?," *J. Biomech.*, vol. 28, no. 6, pp. 753–758, Jun. 1995.

[8] E. M. Figueiredo, G. B. Ferreira, R. C. Maia Moreira, R. N. Kirkwood, and L. Fetters, "Efficacy of Ankle-Foot Orthoses on Gait of Children with Cerebral Palsy: Systematic Review of Literature," *Pediatr. Phys. Ther.*, vol. 20, no. 3, p. 207, Fall 2008, doi: 10.1097/PEP.0b013e318181fb34.

[9] B. Chen, B. Zi, Y. Zeng, L. Qin, and W.-H. Liao, "Ankle-foot orthoses for rehabilitation and reducing metabolic cost of walking: Possibilities and challenges," *Mechatronics*, vol. 53, Feb. 2018, doi: 10.1016/j.mechatronics.2018.06.014.

[10] A. Daryabor, M. Arazpour, and G. Aminian, "Effect of different designs of ankle-foot orthoses on gait in patients with stroke: A systematic review," *Gait Posture*, vol. 62, pp. 268–279, 2018, doi: 10.1016/j.gaitpost.2018.03.026.

[11] Y. L. Kerkum, A. I. Buizer, J. C. van den Noort, J. G. Becher, J. Harlaar, and M.-A. Brehm, "The Effects of Varying Ankle Foot Orthosis Stiffness on Gait in Children with Spastic Cerebral Palsy Who Walk with Excessive Knee Flexion," *PLOS ONE*, vol. 10, no. 11, p. e0142878, Nov. 2015, doi: 10.1371/journal.pone.0142878.

[12] K. C. C. P. D. P. G. O. C. FAAOMPT, S.-C. Y. P. PhD, M. J. P. Ed.D, and M. M. L. P. PT, *Orthotics and Prosthetics in Rehabilitation, 4e*, 4 edition. St. Louis: Saunders, 2019.

[13] R. G. Burdett, D. Borello-France, C. Blatchly, and C. Potter, "Gait comparison of subjects with hemiplegia walking unbraced, with ankle-foot orthosis, and with Air-Stirrup brace," *Phys. Ther.*, vol. 68, no. 8, pp. 1197–1203, Aug. 1988.

[14] C. Bleyenheuft, G. Caty, T. Lejeune, and C. Detrembleur, "Assessment of the Chignon® dynamic ankle–foot orthosis using instrumented gait analysis in hemiparetic adults," *Ann. Réadapt. Médecine Phys.*, vol. 51, no. 3, pp. 154–160, Apr. 2008, doi: 10.1016/j.annrmp.2007.12.005.

[15] S. Fatone and A. H. Hansen, "Effect of ankle-foot orthosis on roll-over shape in adults with hemiplegia," *J. Rehabil. Res. Dev.*, vol. 44, no. 1, pp. 11–20, Jan. 2007.

[16] S. Fatone, S. A. Gard, and B. S. Malas, "Effect of Ankle-Foot Orthosis Alignment and Foot-Plate Length on the Gait of Adults With Poststroke Hemiplegia," *Arch. Phys. Med. Rehabil.*, vol. 90, no. 5, pp. 810–818, May 2009, doi: 10.1016/j.apmr.2008.11.012.

[17] S. J. Mulroy, V. J. Eberly, J. K. Gronely, W. Weiss, and C. J. Newsam, "Effect of AFO Design on Walking after Stroke: Impact of Ankle Plantar Flexion Contracture," *Prosthet. Orthot. Int.*, vol. 34, no. 3, pp. 277–292, Sep. 2010, doi: 10.3109/03093646.2010.501512.

[18] H. Gök, A. Küçükdeveci, H. Altinkaynak, G. Yavuzer, and S. Ergin, "Effects of ankle-foot orthoses on hemiparetic gait," *Clin. Rehabil.*, vol. 17, no. 2, pp. 137–139, Mar. 2003, doi: 10.1191/0269215503cr605oa.

[19] "Ankle-Foot Orthosis (AFO)," *Cascade Orthotics Calgary*. https://www.cascadeorthotics.com/ankle-foot-orthosis-afo-cascade-orthotics/ (accessed Dec. 18, 2019).

[20] P. M. Nair, K. L. Rooney, S. A. Kautz, and A. L. Behrman, "Stepping with an ankle foot orthosis re-examined: a mechanical perspective for clinical decision making," *Clin. Biomech. Bristol Avon*, vol. 25, no. 6, pp. 618–622, Jul. 2010, doi: 10.1016/j.clinbiomech.2010.03.001.

[21] J. F. Lehmann, P. C. Esselman, M. J. Ko, J. C. Smith, B. J. deLateur, and A. J. Dralle, "Plastic ankle-foot orthoses: evaluation of function," *Arch. Phys. Med. Rehabil.*, vol. 64, no. 9, pp. 402–407, Sep. 1983.

[22] "OTC 1705 Posterior Leaf Spring Ankle-Foot Orthosis (A.F.O.) (trimmed)," *LifeSupply.ca - Canada's Wellness Shopping Destination*. https://www.lifesupply.ca/otc-1705-posterior-leaf-spring-ankle-foot-orthosis-a-f-o-trimmed/ (accessed Mar. 18, 2020).

[23] J. C. Patzkowski, R. V. Blank, J. G. Owens, J. M. Wilken, J. A. Blair, and J. R. Hsu, "Can an Ankle-Foot Orthosis Change Hearts and Minds?," ARMY INST OF SURGICAL

RESEARCH FORT SAM HOUSTON TX, Jan. 2011. Accessed: Aug. 20, 2019. [Online]. Available: https://apps.dtic.mil/docs/citations/ADA615271.

[24] A. Bartonek, M. Eriksson, and E. M. Gutierrez-Farewik, "A new carbon fibre spring orthosis for children with plantarflexor weakness," *Gait Posture*, vol. 25, no. 4, pp. 652–656, 2007, doi: 10.1016/j.gaitpost.2006.07.013.

[25] S. I. Wolf, M. Alimusaj, O. Rettig, and L. Döderlein, "Dynamic assist by carbon fiber spring AFOs for patients with myelomeningocele," *Gait Posture*, vol. 28, no. 1, pp. 175–177, Jul. 2008, doi: 10.1016/j.gaitpost.2007.11.012.

[26] "Dynamic User Stories—Iceross Seal-In®, Rheo Knee®, and Pro-Flex®. Ossur.com." https://www.ossur.com/en-us/bracing-and-supports/foot-and-ankle/afo-leaf-spring (accessed Dec. 18, 2019).

[27] A. Wach, "Mechanical Characterization of Carbon Fiber and Thermoplastic Ankle Foot Orthoses," *Masters Theses 2009 -*, Oct. 2015, [Online]. Available: https://epublications.marquette.edu/theses_open/341.

[28] K. Desloovere *et al.*, "How can push-off be preserved during use of an ankle foot orthosis in children with hemiplegia? A prospective controlled study," *Gait Posture*, vol. 24, no. 2, pp. 142–151, 2006, doi: 10.1016/j.gaitpost.2006.08.003.

[29] Å. Bartonek, M. Eriksson, and E. M. Gutierrez-Farewik, "Effects of carbon fibre spring orthoses on gait in ambulatory children with motor disorders and plantarflexor weakness," *Dev. Med. Child Neurol.*, vol. 49, no. 8, pp. 615–620, 2007, doi: 10.1111/j.1469-8749.2007.00615.x.

[30] J. Patzkowski *et al.*, "Comparative Effect of Orthosis Design on Functional Performance," *J. Bone Jt. Surg.*, vol. 94, no. 6, pp. 507–515, Mar. 2012, doi: 10.2106/JBJS.K.00254.

[31] M. J. Highsmith *et al.*, "Outcomes associated with the Intrepid Dynamic Exoskeletal Orthosis (IDEO): A systematic review of the literature," *Mil. Med.*, vol. 181, pp. 69–76, 2016, doi: 10.7205/MILMED-D-16-00280.

[32] K. Bedigrew *et al.*, "Can an Integrated Orthotic and Rehabilitation Program Decrease Pain and Improve Function After Lower Extremity Trauma?," *Clin. Orthop. Relat. Res.*, vol. 472, no. 10, pp. 3017–3025, 2014, doi: 10.1007/s11999-014-3609-7.

[33] "Dynamic Strut AFO." http://www.coyotedesign.com/dynamic-strut-afo.html (accessed Mar. 16, 2020).

[34] J. A. (Joaquin A. Blaya, "Force-controllable ankle foot orthosis (AFO) to assist drop foot gait," Thesis, Massachusetts Institute of Technology, 2002.

[35] J. A. Blaya and H. Herr, "Adaptive control of a variable-impedance ankle-foot orthosis to assist drop-foot gait," *IEEE Trans. Neural Syst. Rehabil. Eng.*, vol. 12, no. 1, pp. 24–31, Mar. 2004, doi: 10.1109/TNSRE.2003.823266.

[36] B. Fournier, "Model and Characterization of a Passive Biomimetic Ankle for Lower Extremity Powered Exoskeleton," Thesis, Université d'Ottawa / University of Ottawa, 2018.

[37] J. D. Carlson and M. R. Jolly, "MR fluid, foam and elastomer devices," *Mechatronics*, vol. 10, no. 4, pp. 555–569, Jun. 2000, doi: 10.1016/S0957-4158(99)00064-1.

[38] H. Naito, Y. Akazawa, K. Tagaya, T. Matsumoto, and M. Tanaka, "An Ankle-Foot Orthosis with a Variable-Resistance Ankle Joint Using a Magnetorheological-Fluid Rotary Damper," *J. Biomech. Sci. Eng.*, vol. 4, no. 2, pp. 182–191, 2009, doi: 10.1299/jbse.4.182.

[39] T. Kikuchi, S. Tanida, K. Otsuki, T. Yasuda, and J. Furusho, "Development of third-generation intelligently Controllable ankle-foot orthosis with compact MR fluid brake," in *2010 IEEE International Conference on Robotics and Automation*, May 2010, pp. 2209–2214, doi: 10.1109/ROBOT.2010.5509729.

[40] F. Ahmadkhanlou, J. L. Zite, and G. N. Washington, "A magnetorheological fluid-based controllable active knee brace," in *Industrial and Commercial Applications of Smart Structures Technologies 2007*, Apr. 2007, vol. 6527, p. 65270O, doi: 10.1117/12.715902.

[41] J. D. Carlson, W. Matthis, and J. R. Toscano, "Smart prosthetics based on magnetorheological fluids," in *Smart Structures and Materials 2001: Industrial and Commercial Applications of Smart Structures Technologies*, Jun. 2001, vol. 4332, pp. 308–316, doi: 10.1117/12.429670.

[42] D. H. Wang and W. H. Liao, "Magnetorheological fluid dampers: a review of parametric modelling," *Smart Mater. Struct.*, vol. 20, no. 2, p. 023001, Jan. 2011, doi: 10.1088/0964-1726/20/2/023001.

[43] S. Tanida *et al.*, "Intelligently controllable Ankle Foot Orthosis (I-AFO) and its application for a patient of Guillain-Barre syndrome," in *2009 IEEE International Conference on Rehabilitation Robotics*, Jun. 2009, pp. 857–862, doi: 10.1109/ICORR.2009.5209590.

[44] J. Furusho *et al.*, "Development of Shear Type Compact MR Brake for the Intelligent Ankle-Foot Orthosis and Its Control; Research and Development in NEDO for Practical Application of Human Support Robot," in *2007 IEEE 10th International Conference on Rehabilitation Robotics*, Jun. 2007, pp. 89–94, doi: 10.1109/ICORR.2007.4428411.

[45] T. Kikuchi, S. Tanida, T. Yasuda, and T. Fujikawa, "Development of control model for intelligently controllable ankle-foot orthosis," in *2013 35th Annual International Conference of the IEEE Engineering in Medicine and Biology Society (EMBC)*, Jul. 2013, pp. 330–333, doi: 10.1109/EMBC.2013.6609504.

[46] D. P. Ferris, K. E. Gordon, G. S. Sawicki, and A. Peethambaran, “An improved powered ankle–foot orthosis using proportional myoelectric control,” *Gait Posture*, vol. 23, no. 4, pp. 425–428, Jun. 2006, doi: 10.1016/j.gaitpost.2005.05.004.

[47] S. J. Smiley, F. S. Jacobsen, C. Mielke, R. Johnston, C. Park, and G. J. Ovaska, “A comparison of the effects of solid, articulated, and posterior leaf-spring ankle-foot orthoses and shoes alone on gait and energy expenditure in children with spastic diplegic cerebral palsy,” *Orthopedics*, vol. 25, no. 4, pp. 411–415, Apr. 2002.

[48] “Trends and techniques in materials, part I: O&P | Lower Extremity Review Magazine.” https://lermagazine.com/article/trends-and-techniques-in-materials-part-i-op (accessed Sep. 13, 2020).

[49] D. A. Winter, *Biomechanics and motor control of human gait: normal, elderly and pathological - 2nd edition*, vol. Ed2. 1991.

[50] J. Perry, S. T. K, and J. R. Davids, “Gait Analysis: Normal and Pathological Function,” *J. Pediatr. Orthop.*, vol. 12, no. 6, p. 815, Dec. 1992.

[51] “tieshoes - chiles19932.” https://sites.google.com/site/chiles19932/tieshoes (accessed Apr. 14, 2020).

[52] “The design and control of active ankle-foot orthoses - ProQuest.” https://search.proquest.com/docview/901460183?pq-origsite=primo (accessed Jun. 12, 2019).

[53] S. C. Walpole, D. Prieto-Merino, P. Edwards, J. Cleland, G. Stevens, and I. Roberts, “The weight of nations: an estimation of adult human biomass,” *BMC Public Health*, vol. 12, no. 1, p. 439, Jun. 2012, doi: 10.1186/1471-2458-12-439.

[54] M. A. McDowell, C. D. Fryar, C. L. Ogden, and K. M. Flegal, “Anthropometric Reference Data for Children and Adults: United States, 2003-2006: (623932009-001).” American Psychological Association, 2008, doi: 10.1037/e623932009-001.

[55] “How Often Do I Need to Change My Orthotics? | Applied Biomechanics,” *Applied Biomechanics Orthotics and Bracing*, Dec. 12, 2014. https://appliedbiomechanics.com/orthotics-bracing-blog/often-need-change-orthotics/ (accessed Mar. 14, 2019).

[56] C. Tudor-Locke *et al.*, “How many steps/day are enough? for adults,” *Int. J. Behav. Nutr. Phys. Act.*, vol. 8, p. 79, Jul. 2011, doi: 10.1186/1479-5868-8-79.

[57] K. P. Clark, L. J. Ryan, and P. G. Weyand, “A general relationship links gait mechanics and running ground reaction forces,” *J. Exp. Biol.*, vol. 220, no. 2, pp. 247–258, Jan. 2017, doi: 10.1242/jeb.138057.

[58] S. A. Bus, “Ground reaction forces and kinematics in distance running in older-aged men,” *Med. Sci. Sports Exerc.*, vol. 35, no. 7, pp. 1167–1175, Jul. 2003, doi: 10.1249/01.MSS.0000074441.55707.D1.

[59] S. Logan, I. Hunter, J. T. J. T. Hopkins, J. B. Feland, and A. C. Parcell, “Ground Reaction Force Differences Between Running Shoes, Racing Flats, and Distance Spikes in Runners.,” *J. Sports Sci. Med.*, vol. 09, no. 1, pp. 147–153, Mar. 2010.

[60] “Slope Steepness Index.” https://geographyfieldwork.com/SlopeSteepnessIndex.htm (accessed Jun. 27, 2020).

[61] M. S. Redfern and J. DiPasquale, “Biomechanics of descending ramps,” *Gait Posture*, vol. 6, no. 2, pp. 119–125, Oct. 1997, doi: 10.1016/S0966-6362(97)01117-X.

[62] R. C. Juvinall, *Fundamentals of Machine Component Design, 5th Edition*, 5 edition. Wiley, 2011.

[63] Budynas, *Shigley’s Mechanical Engineering Design*, 10 edition. SEM, 2014.

[64] C. R. Mischke, “Prediction of Stochastic Endurance Strength,” *J. Vib. Acoust. Stress Reliab. Des.*, vol. 109, no. 1, p. 113, 1987, doi: 10.1115/1.3269383.

[65] H. J. Grover, S. A. Gordon, L. R. Jackson, B. M. Institute, and U. S. B. of N. Weapons, *Fatigue of metals and structures*, Rev. Washington, U.S. Govt. Print. Off., 1960, 1960.

[66] M.-Y. Oh-Park, J. Chacko, and D. D. Kim, “Poster 299: Off-Loading Effect of Patella-Tendon-Bearing Ankle Foot Orthosis in Patients With Diabetic Charcot Neuroarthropathic Foot: A Pilot Study With 12 Months Follow-Up,” *Arch. Phys. Med. Rehabil.*, vol. 89, no. 11, pp. e119–e120, Nov. 2008, doi: 10.1016/j.apmr.2008.09.303.

[67] M. L. Sharp, *Fatigue Design of Aluminum Components and Structures*. McGraw-Hill, 1996.

[68] “Factory Services;” https://www.instron.co.uk/Service and Support/Services/Calibration and Verification/Return to Laboratory (accessed Oct. 07, 2020).

[69] “Overview of materials for Epoxy Cure Resin.” http://www.matweb.com/search/datasheet_print.aspx?matguid=956da5edc80f4c62a72c15ca2b923494 (accessed Oct. 14, 2020).

[70] M. Altin Karataş and H. Gökkaya, “A review on machinability of carbon fiber reinforced polymer (CFRP) and glass fiber reinforced polymer (GFRP) composite materials,” *Def. Technol.*, vol. 14, no. 4, pp. 318–326, Aug. 2018, doi: 10.1016/j.dt.2018.02.001.

[71] E. D. Lemaire, M. D. Tundo, and N. Baddour, “Evaluation of a Smartphone-based Human Activity Recognition System in a Daily Living Environment,” *JoVE J. Vis. Exp.*, no. 106, p. e53004, Dec. 2015, doi: 10.3791/53004.

Appendix A: Technical drawings of designed QRM components

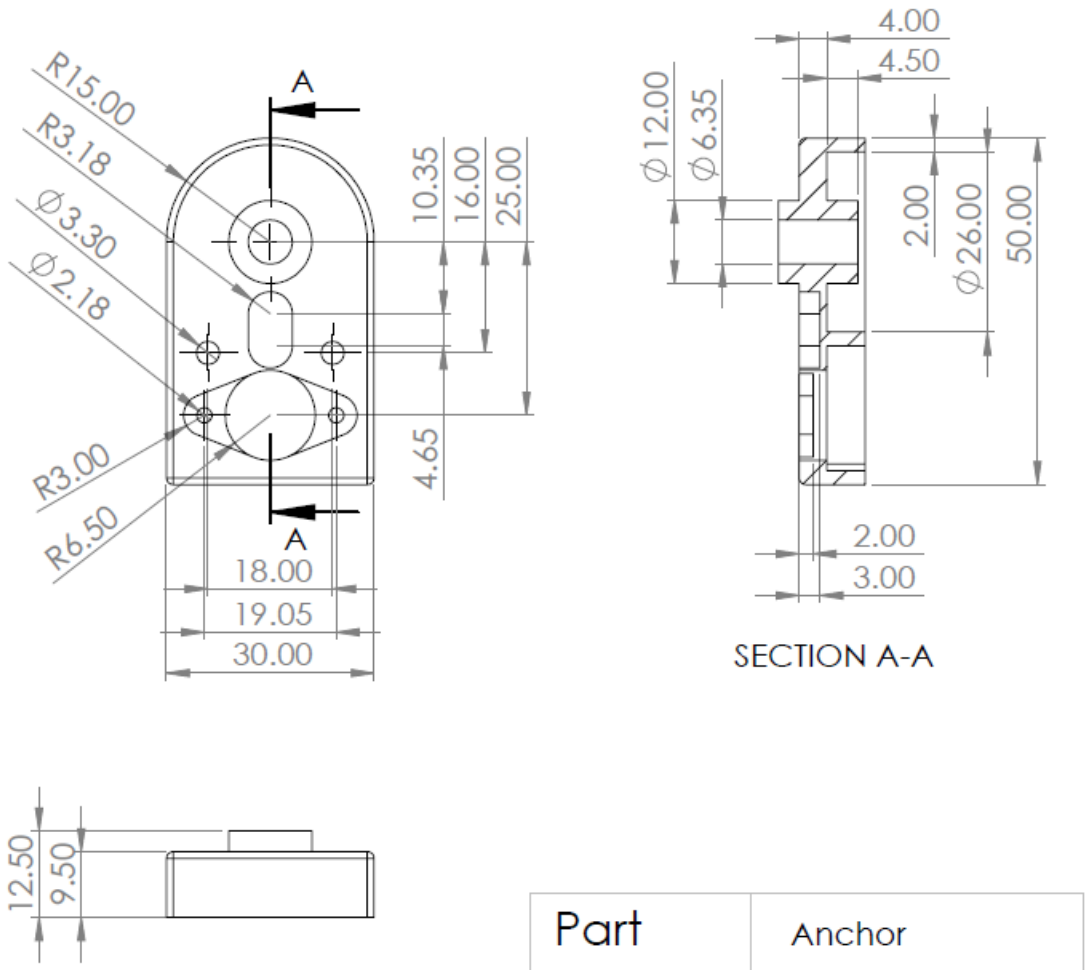

Part	Anchor
Scale	1:1
Material	Aluminum

Figure A-0-1. Technical drawing of anchor

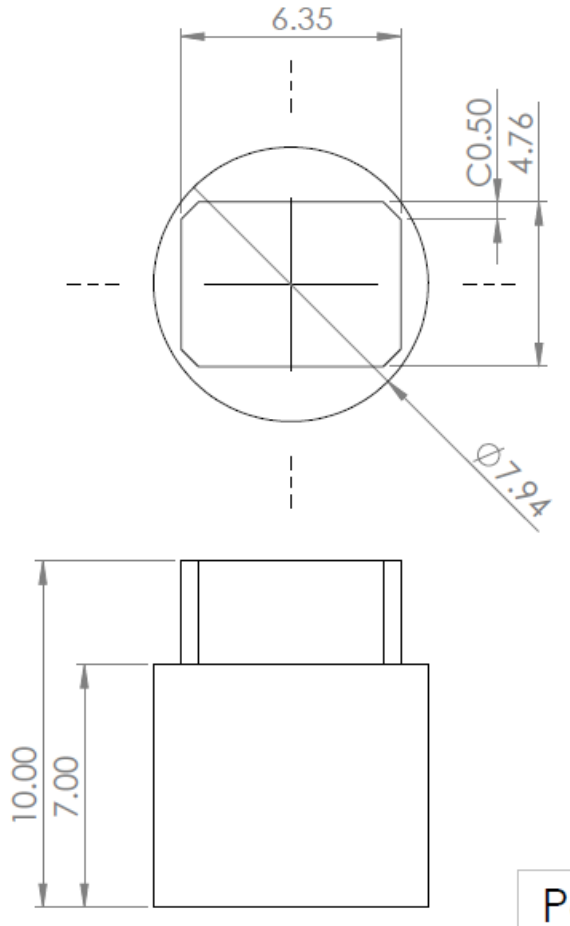

Part	Immobilization pin
Scale	5:1
Material	Acetal

Figure A-0-2. Technical drawing of immobilization pin

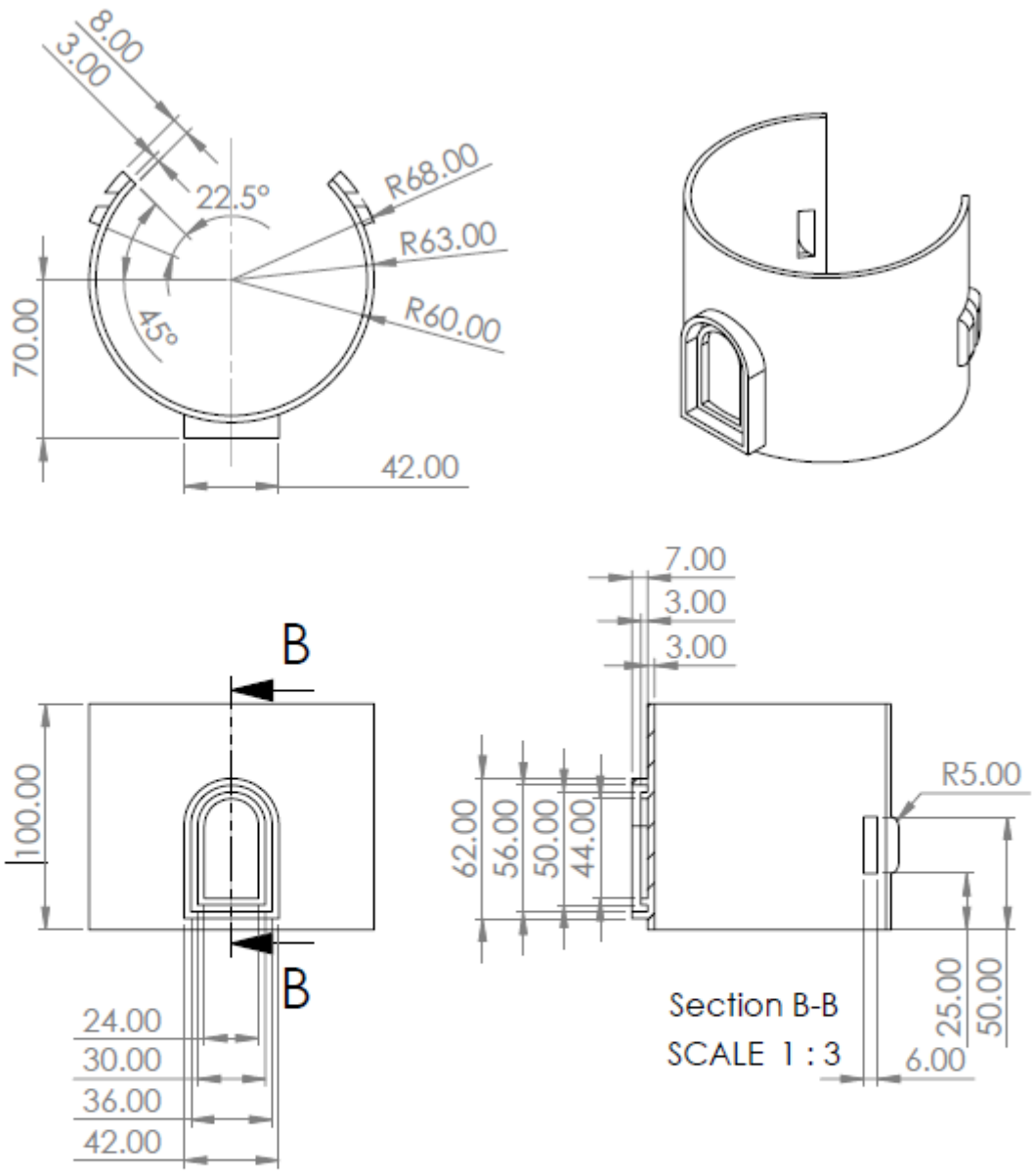

Part	3D printing shank
Scale	1:3
Material	PLA

Figure A-0-3. Technical drawing of 3D printing shank

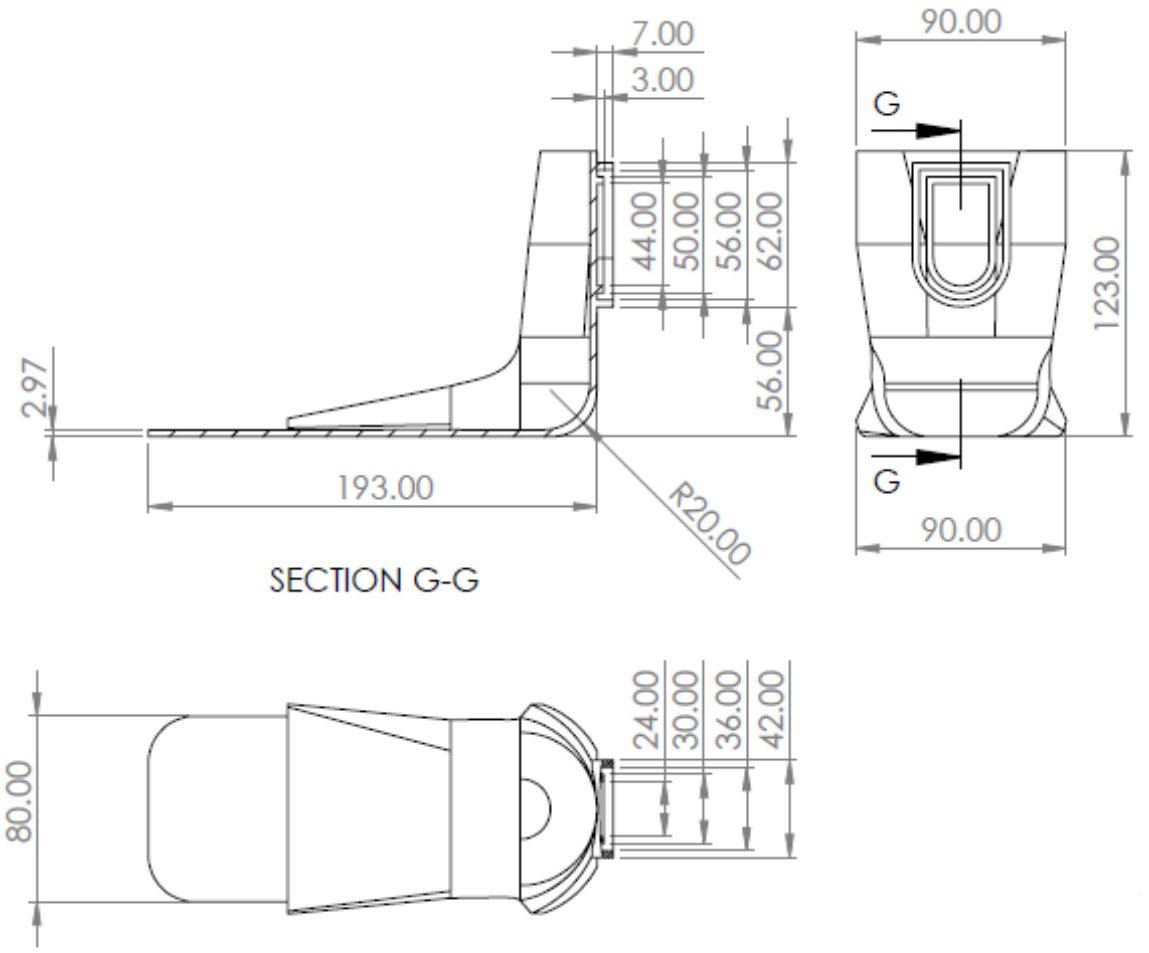

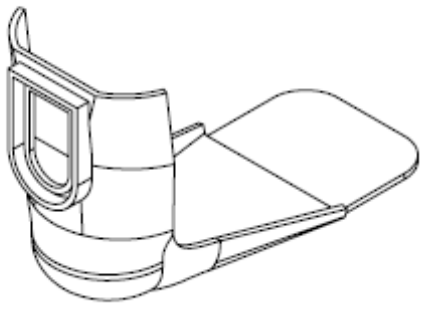

Part	3D printing sole
Scale	1:3
Material	PLA

Figure A-0-4. Technical drawing of 3D printing sole

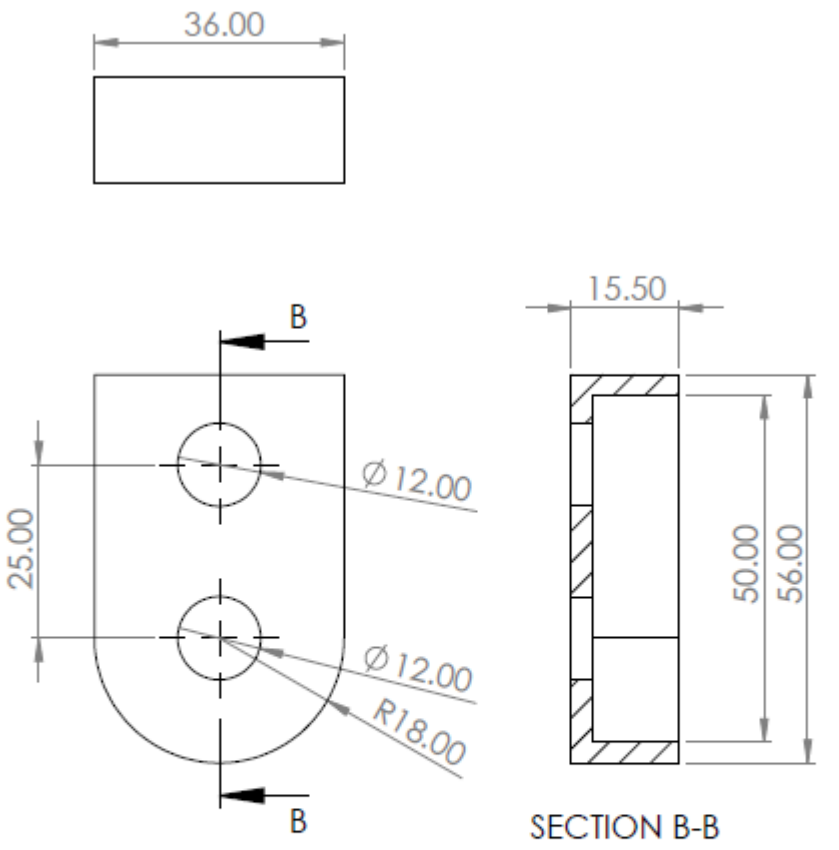

Part	Snap shell
Scale	1:1
Material	PLA

Figure A-0-5. Technical drawing of 3D printing snap shell

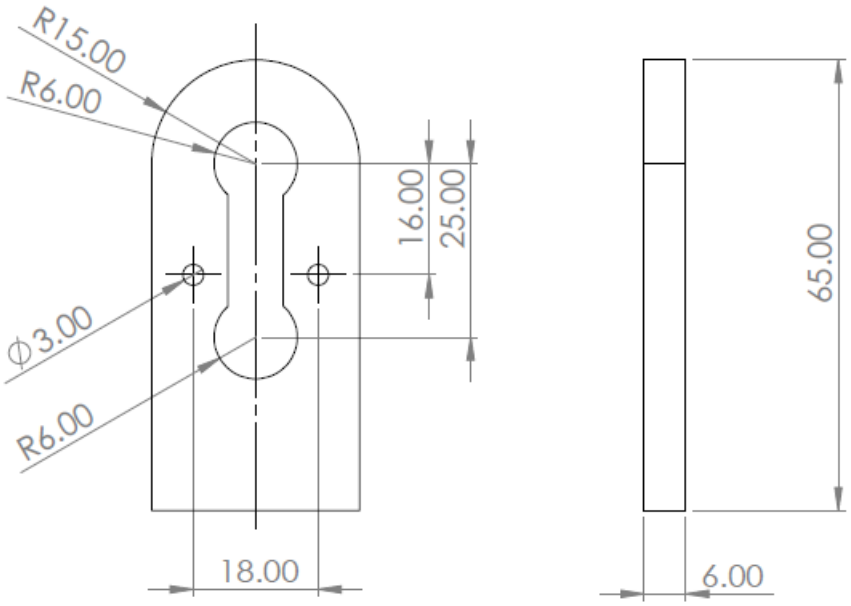

Part	Dummy plate(strut)
Scale	1:1
Material	Acrylic

Figure A-0-6. Technical drawing of strut dummy plate

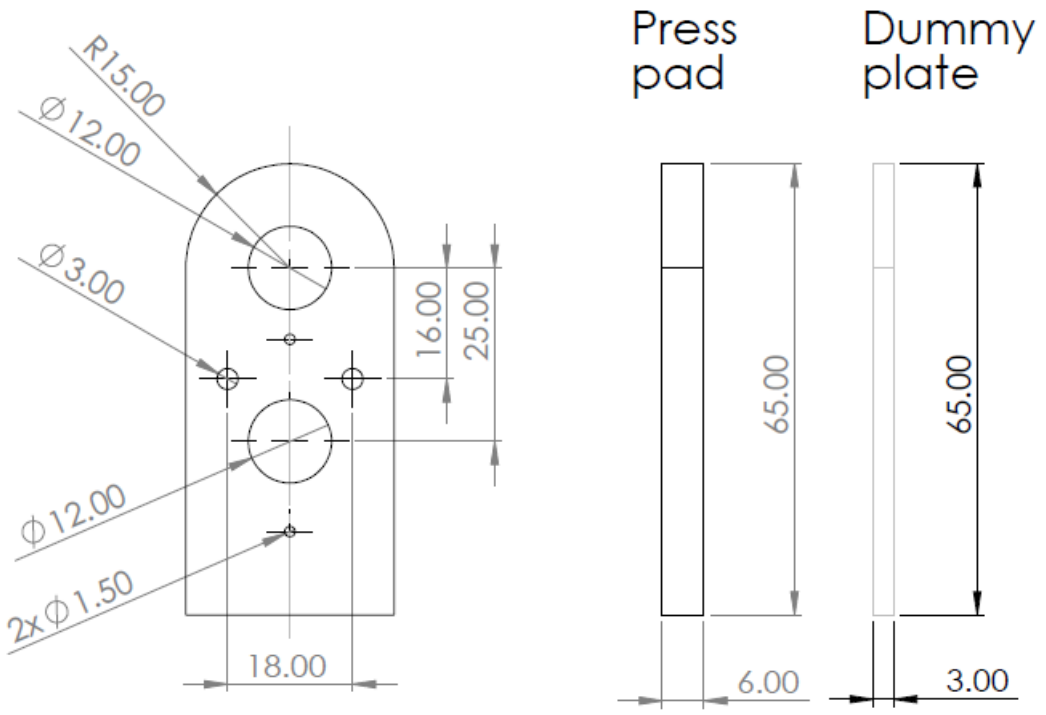

Part	Press pad & Dummy plate
Scale	1:1
Material	Acrylic

Figure A-0-7. Technical drawing of strut lamination dummy plate and press pad

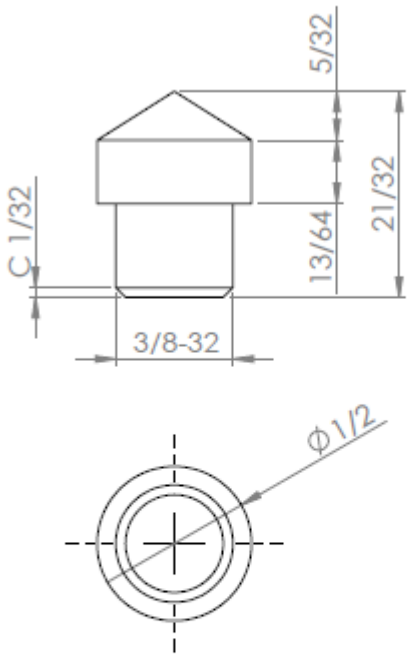

Dimensions are in inches

Part	Receptacle sealer
Scale	2:1
Material	Acetal

Figure A-0-8. Technical drawing of receptacle introducer

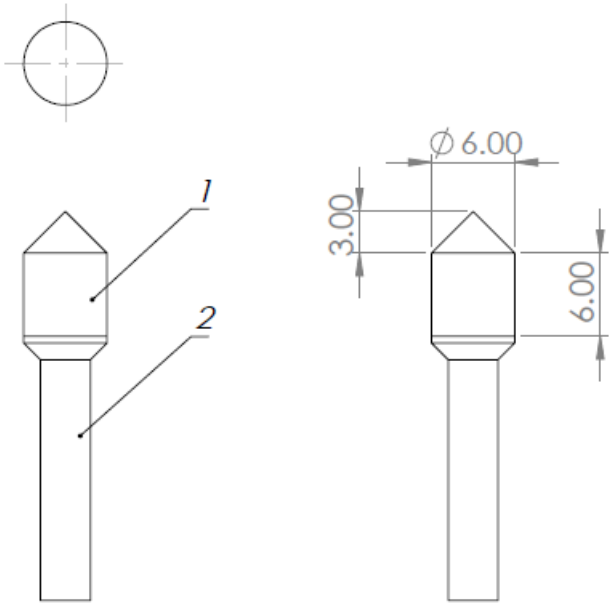

Assemblage		Thread presser	
Parts	1. guider	Material	PLA
	2. machine screw	Size	6-32x3/4
Scale	2:1		

Figure A-0-9. Technical drawing of fixer introducer

Appendix B: Purchased parts specifications

Grade 5 titanium Clevis Pin

Company name:	Allied Titanium, Inc.
Trademark	True Titanium TM.
Part number:	0020207
Material:	Ti-6Al-4V
Finish type:	Machined and polished
Yielding strength:	880 MPa
Ultimate strength:	990 Mpa

Quick release key

Company name:	Skybolt Aeromotive Co.
Trademark:	CLoc
Part number:	ZG2600R2
Material:	Aluminum 6061
Tensile workload:	200 lbs
Shear workload:	200 lbs
Ultimate strength:	300 lbs plus

Receptacle

Company name:	Skybolt Aeromotive Co.
Trademark:	CLoc
Part number:	SK213-2
Material:	Aluminum 6061
Finish type:	Machined
Installation option:	3/32 rivet

Appendix C: Activities circuit list

Following shows an activity circuit [71] to evaluate QRAFO performance in daily activity:

- Start from sitting at a table in uOttawa SITE building (level 1 lobby) with a lower stiffness strut on the QRAFO.
- Stand up and walk 25m across the lobby to a microwave, open and close the microwave door, turn and walk back to the seat and sit down.
- Swap QRAFO to the stiff strut.
- Stand still for 30 seconds.
- Pick up a 40-pound backpack from the table.
- Walk through the connection walkway to the uOttawa CBY building level 1 lobby (55m).
- Walk upstairs to the second floor of CBY and go to the couch area.
- Drop the backpack on a sofa.
- Sit on the bar stool for 30 seconds.
- Go to the spot where a 40-pound dumbbell is on the floor.
- Squat, pick up the dumbbell, and stand up.
- Walk with the dumbbell through a door, around the hallway, and to a conference room (CBY A212).
- Place the dumbbell on the floor.
- Sit at a table for 30 seconds.
- Remove the strut and sit for 30 seconds.
- Simulate driving for 30 seconds.
- Swap to the lower stiffness strut.
- Walk to CBY level 2 lobby, find a sofa and sit on it.
- Take the strut off, sitting for 30 seconds.
- Stand up, walk to the table, sit on a bar stool for 30 seconds.
- Swap to the lower stiffness strut.
- Walk to the stairs, walk downstairs to CBY level 1 lobby, and walk outside.
- Walk to the uOttawa STEM building over the uphill slope (52m).
- Walk back towards CBY building over the downhill slope, stopping at the level area between CBY and STEM.

- If able, swap to the stiff strut without sitting, otherwise sit to swap strut.
- Run 20 meters along the flat area beside STEM.
- Jump 5 times.
- Fast walk counterclockwise along a circle with 5-meter radius.
- Fast walk clockwise along a circle with 5-meter radius.
- Rapidly step left and then back to the right, repeat for 5 times.
- Walk back to SITE building.

Appendix D: Quick release AFO questionnaire

Participant #: _____ Date: _____

This questionnaire will help evaluate if the quick release ankle-foot orthosis (QR-AFO) meets user needs.

Part 1: User Information

Sex: _____ Height: _____(cm/in) Weight: _____(kg/lb)

Years wearing an AFO: _____

Part 2: Please rate the following items by circling the appropriate box.

Is the QR-QR-AFO comfortable?	**All the Time**	**Most of the Time**	**About Half the Time**	**Hardly Ever**	**Never**
Walking ability when using your QR-AFO, compared to walking without an QR-AFO	**Much Improved**	**Improved**	**Same**	**Worse**	**Much Worse**
QR-AFO appearance	**Very Good**	**Good**	**Acceptable**	**Poor**	**Very Poor**
Effort when using your QR-AFO, compared to not using a QR-AFO	**Much Less**	**Somewhat Less**	**Same**	**Somewhat More**	**Much More**
How many hours per day do you wear your QR-AFO?	**More than 8**	**6-8**	**4-6**	**2-4**	**0-2**
Where do you use your QR-AFO?	**Work Only**	**Work, Home**	**Work, Home, Social**	**Work, Social**	**Social Only**
Your QR-AFO's weight is	**Very Light**	**Light**	**Not Light or Heavy**	**Heavy**	**Very Heavy**
QR-AFO support	**Very Secure**	**Somewhat Secure**	**Same as Without Orthosis**	**Somewhat Insecure**	**Very Insecure**
QR-AFO support during high intensity activities (jumping, running, etc.)	**Very Secure**	**Somewhat Secure**	**Same as Without Orthosis**	**Somewhat Insecure**	**Very Insecure**
Overall satisfaction with QR-AFO	**Excellent**	**Above average**	**Average**	**Below Average**	**Poor**

	Yes	**No**
Does the QR-AFO catch your clothes?		
Does the QR-AFO soil your clothes?		
Does the QR-AFO make you perspire?		
Does the QR-AFO rub your skin?		

Part 3: Please rate the following items for your QR-AFO by placing a mark (x) in the appropriate box. In the box to the right, please rate the importance of the items for you.

	Very Difficult	Difficult	Neutral	Easy	Very Easy		Unimportant	Important	Very Important
Putting on the QR-AFO									
Removing the QR-AFO									
Putting on your shoe									
Balance									
Standing									
Pulling open a heavy door									
Carrying a heavy object									
Driving a car									
Energetic activities (run, jump, etc.)									
Level walking									
Walking on uneven ground									
Walking up a slope									
Walking down a slope									
Walking up stairs									
Walking down stairs									
Stepping over a sidewalk curb									
Stepping over small obstacles									
Walking with different speeds									

Part 4: QR-AFO Satisfaction

Please rate your satisfaction with the QR-AFO from 1 to 5, where 1= not satisfied and 5= very satisfied. You may also write comments to better explain your answer.

Objectives	Score
Swapping the strut	
Comments:	
Carrying the strut	
Comments:	
Overall satisfaction about the quick release mechanism	
Comments:	
Would you use the QR-AFO as your regular device	
Comments:	

Part 5: Comments

1. When would you anticipate swapping the strut during daily living?

2. For the next design iteration, which features do you wish to see on the QR-AFO?

Appendix E: Certificate of ethics approval

20/01/2020

Université d'Ottawa
Bureau d'éthique et d'intégrité de la recherche

University of Ottawa
Office of Research Ethics and Integrity

CERTIFICAT D'APPROBATION ÉTHIQUE | CERTIFICATE OF ETHICS APPROVAL

Numéro du dossier / Ethics File Number	H-10-19-4767
Titre du projet / Project Title	Performance evaluation on a quick-release ankle-foot orthosis
Type de projet / Project Type	Thèse de maîtrise / Master's thesis
Statut du projet / Project Status	Approuvé / Approved
Date d'approbation (jj/mm/aaaa) / Approval Date (dd/mm/yyyy)	20/01/2020
Date d'expiration (jj/mm/aaaa) / Expiry Date (dd/mm/yyyy)	19/01/2021

Équipe de recherche / Research Team

Chercheur / Researcher	Affiliation	Role
Wentao LI	Département de génie mécanique / Department of Mechanical Engineering	Chercheur Principal / Principal Investigator
Natalie BADDOUR	Département de génie mécanique / Department of Mechanical Engineering	Superviseur / Supervisor
Edward LEMAIRE		Co-superviseur / Co-supervisor

Conditions spéciales ou commentaires / Special conditions or comments

550, rue Cumberland, pièce 154 Ottawa (Ontario) K1N 6N5 Canada
550 Cumberland Street, Room 154 Ottawa, Ontario K1N 6N5 Canada

613-562-5387 • 613-562-5338 • ethique@uOttawa.ca / ethics@uOttawa.ca
www.recherche.uottawa.ca/deontologie | www.recherche.uottawa.ca/ethics

20/01/2020

Université d'Ottawa

Bureau d'éthique et d'intégrité de la recherche

University of Ottawa

Office of Research Ethics and Integrity

Le Comité d'éthique de la recherche (CÉR) de l'Université d'Ottawa, opérant conformément à l'*Énoncé de politique des Trois conseils* (2014) et toutes autres lois et tous règlements applicables, a examiné et approuvé la demande d'éthique du projet de recherche ci-nommé.

L'approbation est valide pour la durée indiquée plus haut et est sujette aux conditions énumérées dans la section intitulée "Conditions Spéciales ou Commentaires". Le formulaire « Renouvellement ou Fermeture de Projet » doit être complété quatre semaines avant la date d'échéance indiquée ci-haut afin de demander un renouvellement de cette approbation éthique ou afin de fermer le dossier.

Toutes modifications apportées au projet doivent être approuvées par le CÉR avant leur mise en place, sauf si le participant doit être retiré en raison d'un danger immédiat ou s'il s'agit d'un changement ayant trait à des éléments administratifs ou logistiques du projet. Les chercheurs doivent aviser le CÉR dans les plus brefs délais de tout changement pouvant augmenter le niveau de risque aux participants ou pouvant affecter considérablement le déroulement du projet, rapporter tout évènement imprévu ou indésirable et soumettre toute nouvelle information pouvant nuire à la conduite du projet ou à la sécurité des participants.

The University of Ottawa Research Ethics Board, which operates in accordance with the *Tri-Council Policy Statement* (2014) and other applicable laws and regulations, has examined and approved the ethics application for the above-named research project.

Ethics approval is valid for the period indicated above and is subject to the conditions listed in the section entitled "Special Conditions or Comments". The "Renewal/Project Closure" form must be completedfour weeks before the above-referenced expiry date to request a renewal of this ethics approval or closure of the file.

Any changes made to the project must be approved by the REB before being implemented, except when necessary to remove participants from immediate endangerment or when the modification(s) only pertain to administrative or logistical components of the project. Investigators must also promptly alert the REB of any changes that increase the risk to participant(s), any changes that considerably affect the conduct of the project, all unanticipated and harmful events that occur, and new information that may negatively affect the conduct of the project or the safety of the participant(s).

Germain ZONGO
Responsable d'éthique en recherche / Protocol Officer
Pour/For **Daniel LAGAREC** Président(e) du/ Chair of the **Comité d'éthique de la recherche en sciences de la santé et sciences / Health Sciences and Sciences Research Ethics Board**

550, rue Cumberland, pièce 154
Ottawa (Ontario) K1N 6N5 Canada

550 Cumberland Street, Room 154
Ottawa, Ontario K1N 6N5 Canada

613-562-5387 • 613-562-5338 • ethique@uOttawa.ca / ethics@uOttawa.ca
www.recherche.uottawa.ca/deontologie | www.recherche.uottawa.ca/ethics